A simple rule for the evolution of fast dispersal at the edge of expanding populations

A simple rule for the evolution of fast dispersal at the edge of expanding populations

Maxime Deforet[1], Carlos Carmona-Fontaine[2], Kirill S. Korolev[3], Joao B. Xavier[1]
[1]Program in Computational and Systems Biology, Memorial Sloan-Kettering Cancer Center, New York, New York
[2]Center for Genomics and Systems Biology, New York University, New York
[3]Department of Physics and Graduate Program in Bioinformatics, Boston University, Boston
Corresponding: deforetm@mskcc.org, xavierj@mskcc.org

Abstract
Evolution by natural selection is commonly perceived as a process that favors those that replicate faster to leave more offspring; nature, however, seem to abound with examples where organisms forgo some replicative potential to disperse faster. When does selection favor invasion of the fastest? Motivated by evolution experiments with swarming bacteria we searched for a simple rule. In experiments, a fast hyperswarmer mutant that pays a reproductive cost to make many copies of its flagellum invades a population of mono-flagellated bacteria by reaching the expanding population edge; a two-species mathematical model explains that invasion of the edge occurs only if the invasive species' expansion rate, v_2, which results from the combination of the species growth rate and its dispersal speed (but not its carrying capacity), exceeds the established species', v_1. The simple rule that we derive, $v_2 > v_1$, appears to be general: less favorable initial conditions, such as smaller initial sizes and longer distances to the population edge, delay but do not entirely prevent invasion. Despite intricacies of the swarming system, experimental tests agree well with model predictions suggesting that the general theory should apply to other expanding populations with trade-offs between growth and dispersal, including non-native invasive species and cancer metastases.

Introduction

Natural selection is commonly perceived as a process that favors species that grow in numbers by reproducing faster and surviving better. In expanding populations, however, species face a choice between allocating resources to growth or to disperse faster (1). Expanding populations consume local resources; the resource availability is highest outside the population range, which creates an advantage to being at the population margin (2). Fast-dispersing species take advantage of this spatial heterogeneity: they take over the edge, cutting-off competitors' access to growth-limiting resources (1, 3). The role of resource limitation in evolutionary processes, such as gene surfing (4) and the founder effect (5), has been analyzed before; however, crucial questions remain: When does natural selection favor dispersal over growth? How much growth can a fast-dispersing species forgo and still be favored by natural selection?

Invasiveness in expanding populations has global implications at many levels (6): non-native species invade due to human introduction and climate change (7), expanding tumors become invasive cancers (8) and antibiotic-resistant bacteria spread due to global travel (9). Predicting the evolution of expanding populations, however, is a non-trivial problem. Dispersal and growth are sometimes under an allocation trade-off where investing in one trait leaves fewer resources available for the other (10-13). Mathematical modeling could help address these complex questions by defining the conditions favoring fast dispersal.

Testing model predictions with field studies in traditional ecology is challenging and experimental manipulation of natural ecosystems is often impractical. The shortage of robust empirical systems to test mathematical models stalls the development of predictive theory. Laboratory experiments with microbes can provide rigorous tests of mathematical models (5, 14-17); microbes have large populations sizes, short generation times, affordable DNA sequencing and—in many cases—tools for genetic engineering. We recently discovered that experimental evolution in swarming colonies of the bacterium *Pseudomonas aeruginosa* leads to the spontaneous evolution of hyperswarmers (18). Hyperswarmer mutants have a single point mutation in a gene called *fleN;* their cells are multiflagellated, and therefore more dispersive. Importantly, the many flagella come at the cost of a slower growth (table S1). *P. aeruginosa* wild-type outcompete hyperswarmers in well-mixed liquid media; hyperswarmers, on the other hand, swarm faster on semi-solid surfaces (19) and outcompete the wild-type in swarming competitions (18).

Here we exploited the differences in growth rate and dispersal between the wild-type *P. aeruginosa* and its hyperswarmer mutant to motivate, and then experimentally test, a mathematical model of invasion in expanding populations. We based our analysis on a well-established principle of spatial expansion in growing populations: the traveling wave derived from the Fisher-Kolmogorov-Petrovsky-Piscunov (F-KPP) equation. The F-KPP equation, in its original form, describes a 1-D monospecies population (20-22). We expanded the F-KPP equation to investigate the conditions favoring invasion of a species with different dispersal and growth rates and solving that two-species system produced a simple rule to determine the outcome of invasion. Somewhat surprisingly, this simple rule had not been proposed before to

the best of our knowledge, despite much theoretical and experimental work in this field. Simulations reveal the conditions at which the rule is applicable, and the time-scales necessary for invasion in biologically relevant situations. Quantitative experiments with *P. aeruginosa* hyperswarmers indicated that our model may predict the evolution of expanding populations in a wide range of biological scenarios.

Results

Modeling swarming in P. aeruginosa *with the F-KPP equation*

P. aeruginosa populations swarm across agar gels containing nutrients and form branched colonies. Bacteria at the branch tips travel at a nearly constant rate by dividing and dispersing (19). Each growing tip consumes resources in its vicinity and thus forms a nutrient gradient (16) that drives a resource-limited growth similar to the F-KPP model. Knowing that cell sizes have a positive correlation with growth (23) we compared the size of cells collected from the tip of a branch with the size of cells collected behind the tip; cells at the tip were longer indicating faster growth at the edge of the population (Fig. S1). We then modeled *P. aeruginosa* swarming as a one-dimensional expanding population according to the F-KPP equation:

$$\frac{\partial u}{\partial t} = ru\left(1 - \frac{u}{K}\right) + D\frac{\partial^2 u}{\partial x^2} \quad (1)$$

where x is space, t is time, u is the local population density, K is the carrying capacity, r is the maximum per-capita growth rate and D quantifies dispersal. Growth and dispersal can obey different laws in nature; for generality the F-KPP equation assumes logistic growth, where the per-capita growth rate decreases linearly as the population density increases, leading to a decrease in resource availability, and assumes Fickian diffusion for dispersal. The F-KPP equation suits the common scenario where regions with excess of nutrients lie outside the population and determine the direction of expansion. The resource availability, represented by $1 - \frac{u}{K}$, is highest outside the population range and growth, represented by $ru(1 - \frac{u}{K})$, occurs mostly at the edge of the population. Eq. (1) has a traveling wave solution, $u(x,t) = u_0(x - vt)$, where the population front travels at a constant expansion rate $v = 2\sqrt{rD}$ and its density increases from the edge with a length-scale $\lambda = \sqrt{D/r}$ (Movie S1 and Fig. S1) (4, 24). In summary, the F-KPP equation—where low-density at the leading edge drives population expansion—has a traveling wave solution where the expansion rate depends on both growth and dispersal, but is independent of the carrying capacity.

A simple rule for the evolution of faster dispersal

Hyperswarmers grow slower in well-mixed liquid media due the cost of synthesizing multiple flagella, but—thanks to their faster dispersal on semi-solid surfaces—outcompete the wild-type in spatially structured environments (18, 19). In semi-solid surfaces lacking spatial structure hyperswarmers are outcompeted, as expected (Fig. S2). At the micrometer scale, an expanding population of hyperswarmers displays patterns of active turbulence typical of dense bacterial suspensions, which is different from the wild-type where cells remain nearly static even

at the tips of swarming tendrils (Movie S2). To gain a better understanding of the competition dynamics in expanding swarming colonies we mixed wild-type bacteria (labeled with a red fluorescent protein) with hyperswarmers (labeled with a green fluorescent protein) at 10:1 ratio; we then used time-lapsed florescence imaging to film the swarming competition (Fig. 1A). The time-lapse showed that hyperswarmers quickly reached the population edge, increasing their dominance as the colony expanded to win the competition (Movie S3).

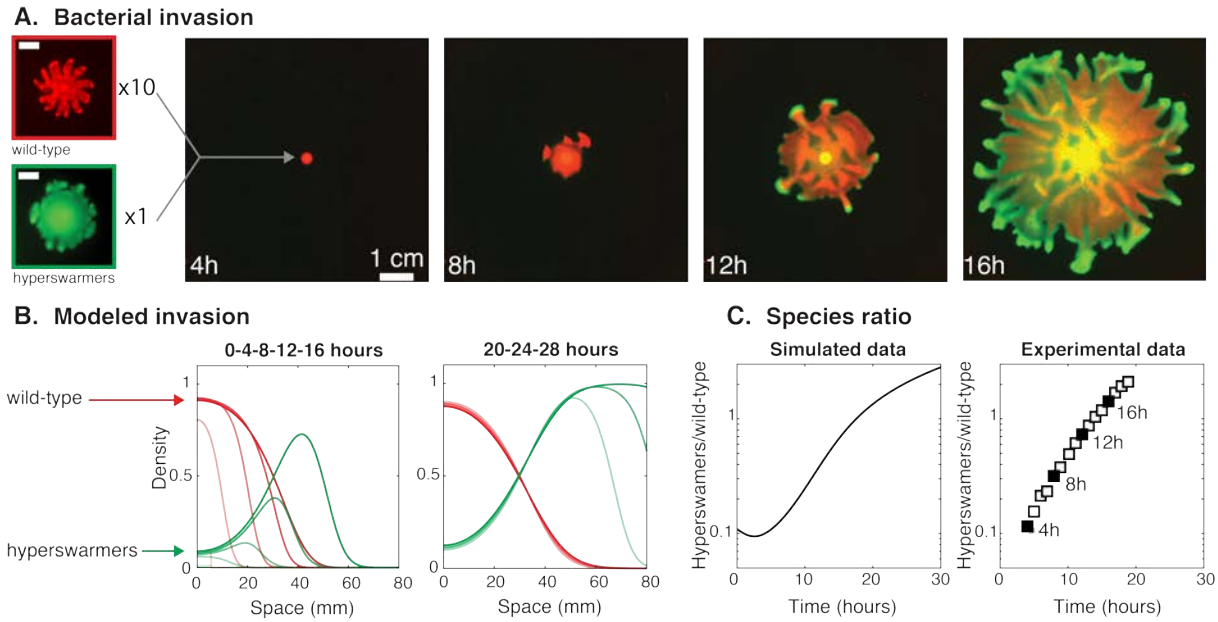

Figure 1: Invasion dynamics in an expanding population of swarming *P. aeruginosa* bacteria. A: Fluorescence time-lapse imaging shows a swarming competition in a mixed population of wild-type and hyperswarmers at 10:1 ratio and on an soft-agar gel. Leftmost panels: Monoclonal swarming colonies of wild-type (top) and hyperswarmer (bottom) imaged at $\boldsymbol{T = 12}$h (scale bars 1 cm). B: Snapshots of numerical simulations of Eq. 2 modeling competition of *P. aeruginosa* (red lines) and the hyperswarmer mutant (green lines) with initial ratio 10:1, using parameters extracted from experiments (Table S1). Left panel shows time points represented in panel A. Right panel shows later time points, where the wild-type population stalls while the hyperswarmer population keeps expanding. C: Ratio of hyperswarmer biomass over wild-type biomass. The experimental data is extracted from fluorescence signals in panel A (black squares represent time points shown in A).

To determine the conditions favoring evolution of faster dispersal we used an extension of the F-KPP equation for a two-species system. Species 1—representing the wild-type—has density function $u_1(x,t)$, disperses with coefficient D_1 and grows with a rate r_1; species 2—representing the hyperswarmer—has $u_2(x,t)$, D_2, and r_2. For simplicity, and according to data for the hyperswarmer system (18) (Fig. S3), we assumed that both species have the same carrying capacity, which we normalized to 1. We assumed that their dispersal rates, determined by D_1 and D_2, are independent.

In this model, the only traits that may be improved in species 2 are its dispersal (D_2) and growth (r_2). The two-species system has two coupled F-KPP equations (25-28):

$$\frac{\partial u_1}{\partial t} = r_1 u_1(1 - u_1 - u_2) + D_1 \frac{\partial^2 u_1}{\partial x^2}$$
$$\frac{\partial u_2}{\partial t} = r_2 u_2(1 - u_1 - u_2) + D_2 \frac{\partial^2 u_2}{\partial x^2} \quad (2)$$

Species 1 and 2 interact only by competing for the same resources, a feature implemented by the factor $1 - u_1 - u_2$. This framework is well established and it was used previously to investigate competition in various contexts of range expansion (17, 25-27, 29-36), including a linear trade-off between dispersal and growth (28). However, previous studies did not continue to derive a general rule to determine the invasion outcome for all possible values of dispersal and growth.

To derive that rule, we first investigated the conditions that allow an introduced population to invade and replace the resident population at the expansion front. We could determine analytically that invasion at the edge occurs only if the expansion rate of species 2 exceeds that of species 1 (see mathematical demonstration in *SI Appendix 2: Analytical solution for the condition of invasion*):

$$v_2 > v_1 \quad (3)$$

where $v_1 = 2\sqrt{r_1 D_1}$ and $v_2 = 2\sqrt{r_2 D_2}$ are the expansion rates of each species when grown alone.

Eq. 3 is a simple rule for invasion of the expansion edge. The intuition behind invasion dynamics is well illustrated in a simulation of the competition between an established species (species 1) and an invader with faster dispersal but slower growth (species 2), which we simulated (Fig. 1B) by numerically solving the system in Eq. 2 with parameters corresponding to the hyperswarmer system ($r_2/r_1 = 0.9$ and $D_2/D_1 = 2$, Table S1). Species 2, initially homogeneously mixed with species 1, outcompetes species 1 once it reaches the leading edge. The invasion succeeds despite the growth disadvantage of species 2 because its faster dispersal enables it to reach the low-density edge where it can take advantage of the resources available. Once species 2 dominates the edge, species 1 is left behind in the high-density region where growth has stopped. Over time, the global frequency of species 1—blocked by species 2 from reaching the edge and incapable of growing further—decreases in frequency whereas species 2 keeps increasing thanks to its edge domination (Fig. 1C, left). These simulation results are consistent with experimental tests conducted here (Fig. 1C, right) and also with the original experiment that led to evolution of hyperswarmers (18), which clearly showed that *fleN* mutants would outcompete the wild-type to extinction given sufficient competition time on swarming plates.

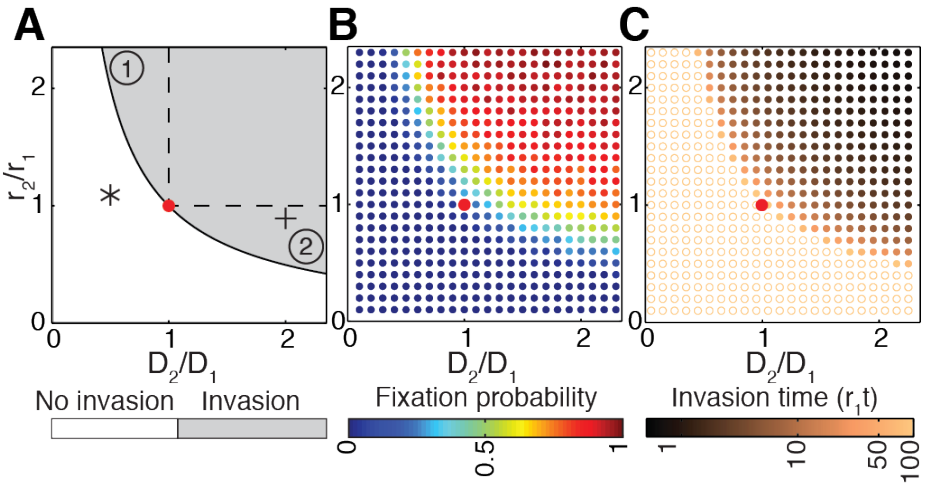

Figure 2. Faster-dispersing species invade expanding populations despite growing slower as long as $v_2 > v_1$. A: Phase diagram of invasion in r_2/r_1, D_2/D_1 space, with 2 subdomains of interest in the invasive domain: (1) is the domain of invasion with lower growth rate and faster dispersal. (2) is the domain of invasion with faster dispersal but lower growth rate. The (+) symbol represents the hyperswarmer phenotype with respect to wild-type phenotype. The (*) symbol represents the wild-type phenotype with respect to the hyperswarmer phenotype. B: Fixation probability obtained from the stochastic model with death rate (stochastic simulations performed with $S = 1$, $K = 100$, $L = 2\lambda_1$). C: Invasion time obtained from the deterministic model (simulations performed with $L = 2\lambda_1$ and $S = 0.2$). The empty orange circles represent absence of invasion within the duration of the simulation ($r_1 t = 180$). In A-C, the red dot depicts the reference point ($D_2 = D_1$ and $r_2 = r_1$).

The invasion rule obtained from the two species system (Eq. 3) states that the evolution of an expanding population is entirely determined from the growth and dispersal rates. Importantly, and similar to the expansion rate obtained for a monospecies traveling wave, the invasion rule is independent of the carrying capacity of each species (See Fig. S4 for confirmation with numerical simulations).

The invasion rule leads to a diagram that delineates the invasion outcome in a growth-dispersal space (Fig. 2A). This diagram shows two trivial domains: when both growth and dispersal of species 2 are lower ($D_2 < D_1$ and $r_2 < r_1$), invasion does not occur because v_2 is always lower than v_1. Numerical simulations explain that for very low values of D_2 and r_2 species 1 continues to expand and travel at constant expansion rate whereas species 2 spreads out and stalls (Movie S4, bottom left panel, and Fig. S5A). When growth and dispersal of species 2 are greater ($D_2 > D_1$ and $r_2 > r_1$), species 2 invades because v_2 is always higher than v_1: species 2 grows rapidly, moves to the front where it reaches the active layer and outcompetes species 1 (Movie S4, top right panel, and Fig. S5B).

The two domains where one trait is higher and the other is lower are less trivial, but arguably more relevant because of the trade-off between dispersal and growth commonly found in nature (6). Domain 1 of Fig. 2A shows that invasion occurs if species 2 disperses slower than species 1 as long as its growth rate is sufficiently higher ($r_2 > r_1 D_1/D_2$, Movie S4, top left panel, and Fig. S5C). Domain 2 shows that species 2 invades even if—like the hyperswarmer—it grows slower than species 1 as long as it disperses fast enough such that $D_2 > D_1 r_1/r_2$. A fast-

dispersing invader reaches the active layer where it can gain better access to growth-limiting resources and outcompete the established species (Movie S4, bottom left panel, and Fig. S5D).

The simple invasion rule, therefore, makes quantitative predictions of invasion outcome that hold true in our experimental system despite intricacies such as the large-scale branching and small-scale turbulence. Hyperswarmers have a ~100% increase in dispersal ($D_2/D_1 \sim 2$) that comes at a ~10% growth rate cost ($r_2/r_1 \sim 0.9$) (Movie S2 and Table S1). Therefore the experimental system falls into domain 2 of the invasion diagram (cross symbol in Fig. 2A).

We measured the frequency of hyperswarmers within the first millimeter of the colony from video frames and saw that it increased exponentially with a rate $\tilde{r} = 0.39 \pm 0.08\,\mathrm{h}^{-1}$, which is in quantitative agreement with the mathematical model (Fig. S6, see Eq. S6 of *SI Appendix 2: Analytical solution for the condition of invasion*). Hyperswarmers introduced into an expanding wild-type colony spread within a wild-type branch (Fig. S7), reach the tip of the branch, and take over the population (Movie S5A) resembling our simulations (Fig. S5D).

Hyperswarmers evolved from a wild-type swarming colony (18) and could take over the ancestral population thanks to a greater dispersal. To test the invasion rule, we asked whether this process was reversible: Could wild-type cells invade the edge of an expanding a hyperswarmer colony thanks to their greater growth rate? Our model predicted that wild-type cells would be unable to invade the hyperswarmer population edge since in this case $v_2 < v_1$ ($D_2/D_1 = 0.5$ and $r_2/r_1 = 1.1$, see star symbol in Fig. 2A). This was confirmed experimentally: wild-type cells introduced in a hyperswarmer colony simply spread out and were rapidly outpaced at the edge by the hyperswarmers (Movie S5B).

Invasion rule valid despite phenotypic variability

Even in mono-species systems, individuals with identical and defined genotypes can still display phenotypic variation (19, 37). To study whether such variation had an effect on invasion outcome, we introduced non-heritable fluctuations in birth and death events as well as in the dispersal processes. These phenotypic variations were modeled as stochastic distributions around the mean population value, which is determined by the strain's genotype (see *SI Appendix 4: Stochastic Modeling*).

Our simulation results show that the invasion rule, $v_2 > v_1$, despite having been derived from deterministic assumptions, holds valid even in stochastic situations. The transition at $v_2 = v_1$ was, however, more gradual (Fig. 2B and S8): the zone of transition broadened as stochasticity increased because, as expected from other stochastic studies (38, 39), stochasticity allowed for a non-zero probability of deleterious mutants ($v_2 < v_1$) to invade and beneficial mutants ($v_2 > v_1$) had a non-zero probability of failing to invade. Larger carrying capacities lessened the stochastic effects and sharpened the transition zone, again as expected from previous stochastic analyses (38, 39); importantly, however, the rule $v_2 > v_1$ could still predict invasion of the population edge even with different carrying capacities (Fig. S9).

We confirmed the generality of the invasion rule further by carrying out evolutionary simulations where mutations randomly arise at division. We considered two schemes: i)

mutations that change growth and/or dispersal relative to the ancestor phenotype but do so in an uncorrelated way; ii) mutations that change growth and dispersal considering that the two traits are linearly correlated (linear trade-off) but independent of the ancestor phenotype. In the case of uncorrelated mutations, populations evolved—on average—towards a greater expansion rate $v = 2\sqrt{rD}$ (Fig. S10C). In contrast, when the two phenotypes were constrained by a trade-off, evolution converged to the value along the trade-off line which maximized the expansion rate $v = 2\sqrt{rD}$ (Fig. S10D-G). In summary, we conducted several types of stochastic simulations that all showed that invasion of the population edge obeys the simple rule $v_2 > v_1$.

The role of spatial structure and founder effect

We then investigated whether our model would account for other factors that can affect invasion and competition in biologically relevant scenarios. For example, in most evolutionary scenarios where competition starts with a mutation the size of the invader population is initially very low (1 individual) whereas a competing species introduced by external processes (e.g. human intervention) can start at higher densities. Also, the initial location of the invader species matters because resources are not evenly distributed in nature, and an invading species may invade faster if it is introduced in the resource-rich leading edge than if it is introduced in deprived regions where it will take longer to grow to domination. In summary, species 2 should take longer to invade (i) when it is introduced further from the edge where resources are already limited or (ii) when its initial size is small. The invasion rule determines whether species 2 can invade (Eq. 3, Fig. 2A) but does not give us the time necessary for invasion.

To investigate how the time to invasion depends on the location and initial size of the invading population we modeled the introduction of species 2 into a traveling wave formed by species 1. We assumed an initial density S across a small interval at a distance L from the edge for species 2 *(SI Appendix 3: Time of invasion*), and we determined the time needed to outnumber species 1 at the front. Numerical simulations revealed that the general rule, $v_2 > v_1$ holds for all initial conditions given sufficient time (Fig. 2C). The time required, however, depends on the initial conditions, increasing approximately linearly with the distance L from the front and decreasing sub-linearly with the initial density S (Fig. S11 and S12).

To better distinguish the factors that influence the time-scale of invasion we considered two steps: first, we considered that species 2 disperses until it reaches the active layer. The time for species 2 to reach the edge depends on the distance from the introduction point to the front—a distance that increases constantly because species 1 is itself advancing—and also on the initial width of species 2. Second, once species 2 reaches the active layer it must grow to outnumber species 1. When the introduction is sufficiently far from the edge the time of invasion, t_i, is:

$$t_i \sim \alpha L - \beta \log(S) \quad (4)$$

where α and β depend on the parameters D_1, D_2, r_1 and r_2 (see *SI Appendix 3: Time of invasion*). This analysis confirms simulation results that the time to invasion depends linearly on L but only sub-linearly on S (Fig. S11 and S12), highlighting that the distance to the edge is key to invasion.

We then tested these findings in our experimental system. We manipulated the distance to

the edge (L) and the density (S) of a small population of hyperswarmers introduced into an expanding wild-type population, and we compared the experimental results to the corresponding simulations. In simulations, the invasion outcome was calculated as the frequency *f* of species 2 at the edge of the population 6 hours after implantation (Fig. 3A). In the experiments, we ranked the invasion outcome after 6 h of expansion as no invasion, scarce invasion, abundant invasion and complete invasion according to the amount of hyperswarmers visible at the edge (Fig. 3B, see details in *SI Appendix 1: Materials and Methods*). The experiments confirmed the dominant role of L compared to S in determining the time of invasion (Eq. 4), which is evident from the concave shape of the invasion scores (Fig. 3C, see *SI Appendix 5: Statistical analysis*).

The intuition behind the concave shape is that when the initial distance from the edge is too long then the invasive species may not be able to invade within biologically relevant time, even if its initial size is large. The shape of the iso-frequency contour lines can be calculated from the simplified two-step model of invasion described above and is given by

$$S \sim e^{L/L_0} \tag{5}$$

where $L_0 = 4D_2 v_1/(3v_1^2 + v_2^2)$ is the characteristic length of theses lines. In the case of *P. aeruginosa* and its hyperswarmers $L_0 = 1.1 \pm 0.07$ mm (SD). The results from our hyperswarmer experiments agree with the theoretical model (Fig. 3A and C; compare to lines of constant mutant frequency), indicating that the two-species F-KPP model, in spite of its simplifying assumptions and despite any intricacies of the experimental system (e.g. the swarming population is tri-dimensional; bacterial cells tend to lose motility as they lose access to resources inside the population, which freezes the spatial organization), is sufficiently general to describe invasion in swarming colonies.

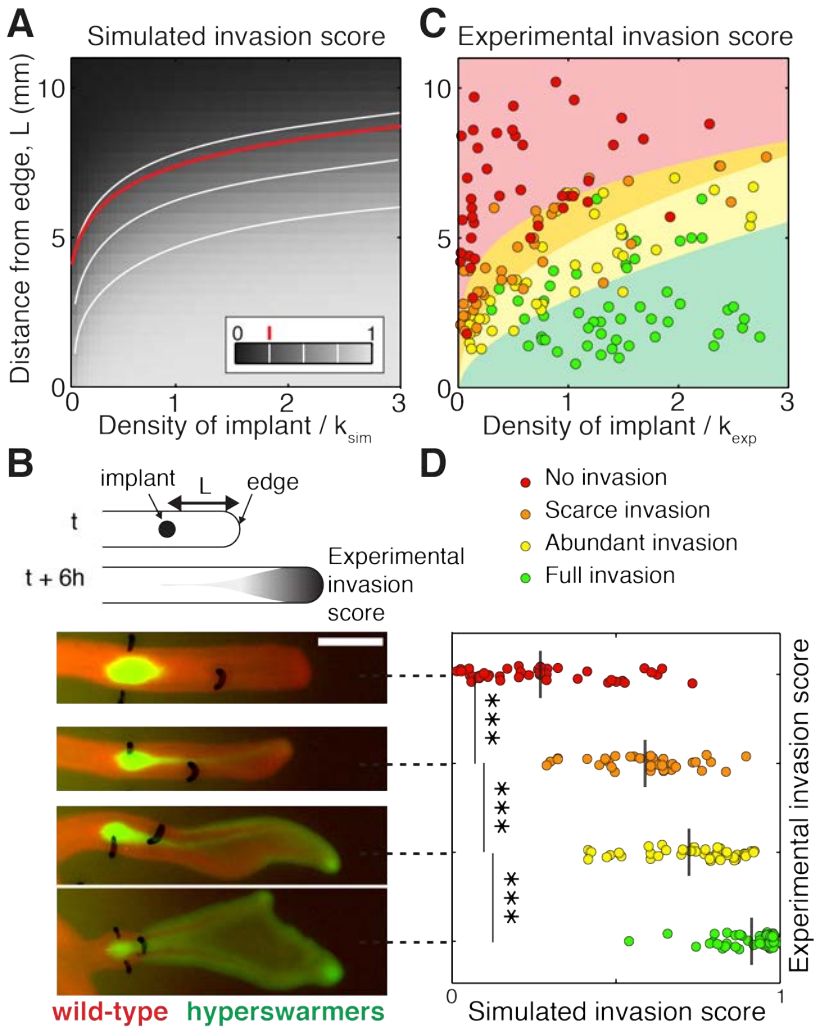

Figure 3. Likelihood of invasion increases with the initial size of the invading population and its proximity to the population edge. A: Simulation results of introducing species 2 into an expanding species 1. The color scale represents the frequency f of the invading species (species 2 with $\boldsymbol{D_2 = 2D_1}$ and $\boldsymbol{r_2 = 0.9r_1}$) at the population edge $\boldsymbol{T = 6h}$ after introduction. White lines are iso-frequency lines for $f = 0.25$, 0.5, and 0.75. The red line is from Eq. (5) for f =0.25. B: Invasion experiments where the hyperswarmer (in green) was introduced at varying initial densities and distances to the edge of an expanding swarm of wild-type *P. aeruginosa* (in red). Scale bar is 5 mm. Leftmost marks depict the location of the hyperswarmer introduction; rightmost marks locate the position of the front of the *P. aeruginosa* population at the time of hyperswarmer implantation. The four snapshots represent four experimental replicates. C: Experimental invasion success evaluated visually at 6 hours after hyperswarmer introduction. Background colors represent results from multinomial logistic regression (see details in *SI Appendix 5: Statistical analysis*). In agreement with the theory, invasion success is lower for large distances from the front and smaller initial densities. D: Comparison of simulated and experimental invasion scores for each experimental replicate. The grey vertical lines represent the average simulated invasion score and the p-values are $< 10^{-3}$ (Kruskal-Wallis test).

Discussion

Since the modern synthesis unified principles of natural selection and genetics in the same mathematical framework, simple rules have provided important solutions to evolutionary puzzles (40). Many cornerstone concepts of evolutionary theory can be expressed as such rules, and their logic can be followed from simplifying assumptions. Real systems are often more complicated, but simple rules still provide useful "rules of thumb" to guide intuition. For instance, Hamilton's rule of kin selection (41), which among other feats determines conditions for the evolution of altruism, drives despite its simplifying assumptions an important body of work both theoretical and experimental in social evolution (42). The F-KPP is one such simple equation to describe the contributions of growth and dispersal to the spatial expansion of a mono-species population (20, 21). The F-KPP also defines conditions for a traveling wave which resembles expanding populations observed in nature, and allows calculating the traveling wave speed from the growth and dispersal rates.

Here we showed that extending the F-KPP equation to a multi-species situations produces a simple mathematical rule to predict the outcome of invasion in an expanding edge depending on the growth and dispersal rates of the competing species. The problem of invasion in an expanding population had been investigated, both theoretically (e.g. 43, 44) and empirically (e.g. 7). But its simple solution, the inequality $v_2 > v_1$, had not been—to the best of our knowledge—presented this way before, a fact that somewhat surprises us.

This simple rule derived analytically from the deterministic two-species F-KPP equation establishes the mutual contribution of growth and dispersal for the invasion outcome. Importantly, the outcome can be independent of the system's carrying capacity, particularly because the competition dynamics relies especially on the low-density of the population at the expanding edge. Further away from the edge, where population is denser, spatial structure and dispersal are less relevant; the evolutionary fate of an invader might then be determined by high-density dynamics where additional factors such as kin competition become important (36, 45). The combined effect of growth and dispersal was also tested experimentally using a laboratory system of swarming bacteria. The rule determined that a slower growing species could invade an established species as long as its dispersal rate is sufficiently faster and that was indeed the case in our experimental system. Hyperswarmer mutants paid a growth cost for synthesizing their multiple flagella but—without affecting their competitive ability—dispersed faster than wild-type bacteria (domain 2 of Fig. 2A).

Our experimental tests with hyperswarmers showed, then, that the invasion rule $v_2 > v_1$ applies to an empirical system despite intricacies that could violate the simplifying assumptions of the F-KPP. This is important, because nature abounds with examples like our experiments where invasive species speed up dispersal but at a cost to their growth rate: the invasion of the cane toads in Australia, a human-introduced species, is led by faster long-legged individuals with lower birth rates (46); the South African mountain fynbos is threatened by invasive pine trees with lighter pine seeds that disperse better (47) but produce weaker seedlings (48); metastatic cancer cells are more invasive due to a loss of contact inhibition of locomotion (49) that also

lowers their cellular proliferation rates (50-53). Additional examples include other plants (54-56), freshwater ciliates (57), bugula (58), fish (59), crickets (60), beetles (61, 62) and butterflies (63). Our invasive rule may potentially be applied to these systems as well, despite their specific intricacies, and used to make quantitative predictions of invasion outcomes.

We should note two exceptions to our findings. First, while our model predicts that a species with faster growth but slower dispersal should be able to invade (domain 1 of Fig. 2A), we did not observe examples of this in our experimental system. And, besides observations by another group in laboratory experiments with *Escherichia coli* (64), we could not find examples in nature either. The reason for not finding invasion of rapid growers that disperse slower may be population history: Empirical and theoretical studies of range expansions suggest that only dispersal can be improved in expanding populations (65-68); invasion of new niches is possibly a rare event, whereas competition within a confined, but relatively homogenous environment is more common. In such situations, the selection is not on dispersal but on growth, which means that—in most species—growth rates may already be close to their physiological limit (Fig. 4A). Individuals challenged to overcome spatial structure may only have dispersal-related traits left to improve. Second, while the trade-off between growth and dispersal may be found and seem logical, a comparative analysis of dispersal in terrestrial and semi-terrestrial animals suggested that dispersal and fecundity may be positively correlated (69).

The trade-off between growth and dispersal likely results from molecular, cellular and physiological constraints, whereas the invasion rule $v_2 > v_1$ specifies the outcome of invasion. The rule determines the maximal cost in growth $|\Delta r|_{\max}$ that the invader can afford to pay for faster dispersal and still be able to dominate the edge of the expanding population (Fig. 4B):

$$|\Delta r|_{\max} = r_1 \left(1 - \frac{D_1}{D_1 + \Delta D}\right) \quad (7)$$

where ΔD is the increase of dispersal in species 2 relatively to species 1. The evolutionary experiment that originally created the hyperswarmers always produced mutations in *fleN*, a gene involved in the regulation of flagellar synthesis (18). It is possible that other mutations could increase dispersal even more, but were not favored if they carried costs higher than $|\Delta r|_{\max}$.

The invasion rule $v_2 > v_1$ could be combined with quantitative knowledge on the physiological mechanisms of a trade-off between growth and dispersal and used to better predict the evolution of expanding populations. For example, if the trade-off can be represented by a line in (r, D) space the slope of that line, dr/dD, represents the cost of dispersal. When the trade-off is subtle, the slope is shallow and we predict that the population will evolve to disperse faster with a lower growth rate (Fig. 4C). Conversely, when the trade-off is strong, the slope is steep and we predict that the population will evolve a higher growth rate and slower dispersal (Fig. 4D). According to this model, the *P. aeruginosa* system has a subtle trade-off: the improved dispersal advantage of hyperswarmers is ~100% but costs only ~10 % of their growth rate relatively to wild-type (18).

Using the simple invasion rule to make predictions about real world scenarios must take into account the appropriate time scales. Our analysis showed that in some conditions where the model predicts invasion, the invasion might take so long that it becomes irrelevant; other

processes—working on shorter time scales—would likely alter the system in the meantime. For example, the hyperswarmers may never invade a real world population of the wild-type if conditions change such that the bacteria need to suddenly form a biofilm. This is particularly important because the same *fleN* mutations that give multiple flagella to hyperswarmers also decreased their ability to form biofilm communities (18). Like Hamilton's rule and other cornerstone concepts of evolutionary theory, if the conditions change dramatically before a fast invader has the chance to dominate the edge of the expanding population then obviously the model predictions will not hold.

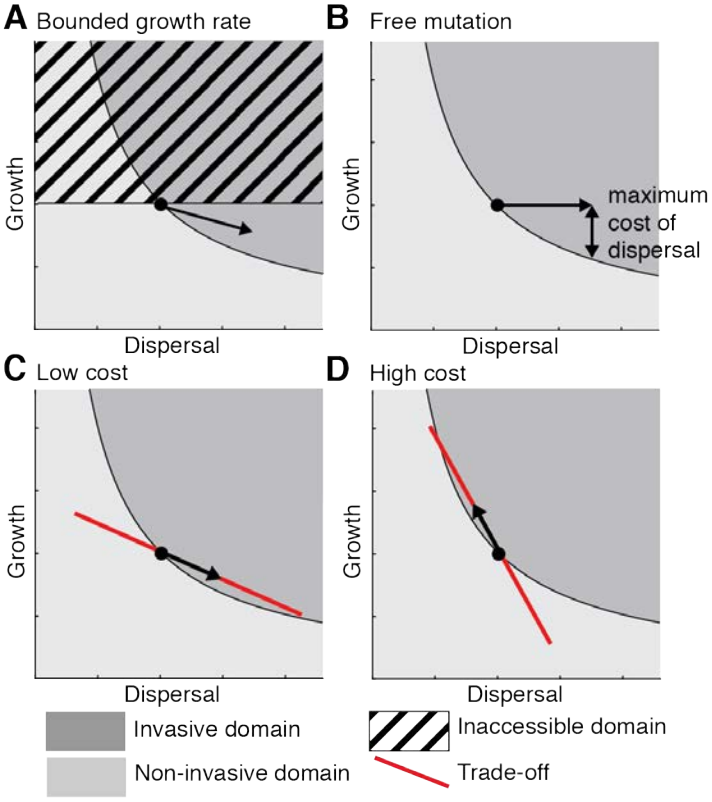

Figure 4. Evolutionary predictions from the invasion diagram in four scenarios. A: the growth rate is bounded by physiology. B: illustration of the maximal cost of an increased dispersal. C and D: linear trade-off between growth and dispersal that corresponds to a low cost of dispersal (C) and high cost of dispersal (D).

In summary, we found a simple rule for invasion that, expanded with trade-off constraints observed for each particular system, could be used to predict the fate of expanding populations. Every model requires simplifying assumptions, and ours is certainly not an exception. In those systems where the rule does hold, the invasion rule could be used to help control expanding populations. Systems in this category may include the growth of cancer tumors and invasion of non-native species in ecosystems.

References

1. Phillips BL, Brown GP, Shine R. Life-history evolution in range-shifting populations. Ecology. 2010;91(6):1617-27.
2. Murray JD. Mathematical biology. 3rd ed. New York: Springer; 2002.
3. Nadell CD, Foster KR, Xavier JB. Emergence of spatial structure in cell groups and the evolution of cooperation. PLoS computational biology. 2010;6(3):e1000716.
4. Hallatschek O, Nelson DR. Gene surfing in expanding populations. Theoretical population biology. 2008;73(1):158-70.
5. Hallatschek O, Hersen P, Ramanathan S, Nelson DR. Genetic drift at expanding frontiers promotes gene segregation. Proceedings of the National Academy of Sciences of the United States of America. 2007;104(50):19926-30.
6. Chuang A, Peterson CR. Expanding population edges: theories, traits, and trade-offs. Global change biology. 2016;22(2):494-512.
7. Phillips BL, Brown GP, Webb JK, Shine R. Invasion and the evolution of speed in toads. Nature. 2006;439(7078):803.
8. Waclaw B, Bozic I, Pittman ME, Hruban RH, Vogelstein B, Nowak MA. A spatial model predicts that dispersal and cell turnover limit intratumour heterogeneity. Nature. 2015;525(7568):261-4.
9. Davies J, Davies D. Origins and evolution of antibiotic resistance. Microbiology and molecular biology reviews : MMBR. 2010;74(3):417-33.
10. Bonte D, Van Dyck H, Bullock JM, Coulon A, Delgado M, Gibbs M, et al. Costs of dispersal. Biological reviews of the Cambridge Philosophical Society. 2012;87(2):290-312.
11. Kneitel JM, Chase JM. Trade-offs in community ecology: linking spatial scales and species coexistence. Ecol Lett. 2004;7(1):69-80.
12. Livingston G, Matias M, Calcagno V, Barbera C, Combe M, Leibold MA, et al. Competition-colonization dynamics in experimental bacterial metacommunities. Nature communications. 2012;3:1234.
13. Tilman D. Competition and Biodiversity in Spatially Structured Habitats. Ecology. 1994;75(1):2-16.
14. Dai L, Korolev KS, Gore J. Slower recovery in space before collapse of connected populations. Nature. 2013;496(7445):355-8.
15. Jessup CM, Kassen R, Forde SE, Kerr B, Buckling A, Rainey PB, et al. Big questions, small worlds: microbial model systems in ecology. Trends in ecology & evolution. 2004;19(4):189-97.
16. Mitri S, Clarke E, Foster KR. Resource limitation drives spatial organization in microbial groups. The ISME journal. 2016;10(6):1471-82.
17. Gandhi SR, Yurtsev EA, Korolev KS, Gore J. Range expansions transition from pulled to pushed waves as growth becomes more cooperative in an experimental microbial population. Proceedings of the National Academy of Sciences. 2016;113(25):6922-7.
18. van Ditmarsch D, Boyle KE, Sakhtah H, Oyler JE, Nadell CD, Deziel E, et al. Convergent evolution of hyperswarming leads to impaired biofilm formation in pathogenic bacteria. Cell reports. 2013;4(4):697-708.
19. Deforet M, van Ditmarsch D, Carmona-Fontaine C, Xavier JB. Hyperswarming adaptations in a bacterium improve collective motility without enhancing single cell motility. Soft matter. 2014;10(14):2405-13.
20. Fisher RA. The wave of advance of advantageous genes. Annals of Eugenics. 1937;7(4):355-69.
21. Kolmogorov A, Petrovskii I, Piscunov N. A study of the equation of diffusion with increase in the quantity of matter, and its application to a biological problem. Byul Moskovskogo Gos Univ. 1937;1(6):1--25.
22. Giometto A, Rinaldo A, Carrara F, Altermatt F. Emerging predictable features of replicated biological invasion fronts. Proceedings of the National Academy of Sciences of the United States of America. 2014;111(1):297-301.

23. Deforet M, van Ditmarsch D, Xavier JB. Cell-Size Homeostasis and the Incremental Rule in a Bacterial Pathogen. Biophysical journal. 2015;109(3):521-8.
24. Murray J. Mathematical Biology: I. An Introduction (Interdisciplinary Applied Mathematics) (Pt. 1): Springer; 2007.
25. Bénichou O, Calvez V, Meunier N, Voituriez R. Front acceleration by dynamic selection in Fisher population waves. Physical Review E. 2012;86(4):041908.
26. Korolev KS. Evolution Arrests Invasions of Cooperative Populations. Physical review letters. 2015;115(20):208104.
27. Pigolotti S, Benzi R, Perlekar P, Jensen MH, Toschi F, Nelson DR. Growth, competition and cooperation in spatial population genetics. Theoretical population biology. 2013;84:72-86.
28. Reiter M, Rulands S, Frey E. Range Expansion of Heterogeneous Populations. Physical review letters. 2014;112(14):148103.
29. Ramanantoanina A, Ouhinou A, Hui C. Spatial assortment of mixed propagules explains the acceleration of range expansion. PloS one. 2014;9(8):e103409.
30. Bouin E, Calvez V, Meunier N, Mirrahimi S, Perthame B, Raoul G, et al. Invasion fronts with variable motility: Phenotype selection, spatial sorting and wave acceleration. Cr Math. 2012;350(15-16):761-6.
31. Lehe R, Hallatschek O, Peliti L. The Rate of Beneficial Mutations Surfing on the Wave of a Range Expansion. PLoS computational biology. 2012;8(3):e1002447.
32. King JR, McCabe PM. On the Fisher-KPP equation with fast nonlinear diffusion. P Roy Soc a-Math Phy. 2003;459(2038):2529-46.
33. Holzer M, Scheel A. Accelerated Fronts in a Two-Stage Invasion Process. Siam J Math Anal. 2014;46(1):397-427.
34. Berestycki H, Coulon AC, Roquejoffre JM, Rossi L. The effect of a line with nonlocal diffusion on Fisher-KPP propagation. Math Mod Meth Appl S. 2015;25(13):2519-62.
35. Lewis MA, Li B, Weinberger HF. Spreading speed and linear determinacy for two-species competition models. Journal of Mathematical Biology. 2002;45(3):219-33.
36. Jong-Shenq G, Chang-Hong W. Dynamics for a two-species competition–diffusion model with two free boundaries. Nonlinearity. 2015;28(1):1.
37. Waite AJ, Frankel NW, Dufour YS, Johnston JF, Long J, Emonet T. Non-genetic diversity modulates population performance. Molecular Systems Biology. 2016;12(12).
38. Otto SP, Whitlock MC. The probability of fixation in populations of changing size. Genetics. 1997;146(2):723-33.
39. Gillespie JH. Population genetics: a concise guide: JHU Press; 2010.
40. Servedio MR, Brandvain Y, Dhole S, Fitzpatrick CL, Goldberg EE, Stern CA, et al. Not Just a Theory—The Utility of Mathematical Models in Evolutionary Biology. PLOS Biology. 2014;12(12):e1002017.
41. Hamilton WD. The genetical evolution of social behaviour. I. Journal of Theoretical Biology. 1964;7(1):1-16.
42. Foster K, Wenseleers T, Ratnieks F. Kin selection is the key to altruism. Trends in ecology & evolution. 2006;21(2):57-60.
43. Burton OJ, Phillips BL, Travis JM. Trade-offs and the evolution of life-histories during range expansion. Ecol Lett. 2010;13(10):1210-20.
44. Phillips BL. Evolutionary processes make invasion speed difficult to predict. Biol Invasions. 2015;17(7):1949-60.
45. Kubisch A, Fronhofer EA, Poethke HJ, Hovestadt T, Associate Editor: Sean HR, Editor: Troy D. Kin Competition as a Major Driving Force for Invasions. The American Naturalist. 2013;181(5):700-6.
46. Hudson CM, Phillips BL, Brown GP, Shine R. Virgins in the vanguard: low reproductive frequency in invasion-front cane toads. Biol J Linn Soc. 2015;116(4):743-7.

47. Richardson DM, Cowling RM, Le Maitre DC. Assessing the risk of invasive success in Pinus and Banksia in South African mountain fynbos. Journal of Vegetation Science. 1990;1(5):629-42.
48. Reich PB, Oleksyn J, Tjoelker MG. Seed Mass Effects on Germination and Growth of Diverse European Scots Pine Populations. Can J Forest Res. 1994;24(2):306-20.
49. Carmona-Fontaine C, Matthews HK, Kuriyama S, Moreno M, Dunn GA, Parsons M, et al. Contact inhibition of locomotion in vivo controls neural crest directional migration. Nature. 2008;456(7224):957-61.
50. Gerlee P, Nelander S. The impact of phenotypic switching on glioblastoma growth and invasion. PLoS computational biology. 2012;8(6):e1002556.
51. Biddle A, Liang X, Gammon L, Fazil B, Harper LJ, Emich H, et al. Cancer stem cells in squamous cell carcinoma switch between two distinct phenotypes that are preferentially migratory or proliferative. Cancer research. 2011;71(15):5317-26.
52. Widmer DS, Cheng PF, Eichhoff OM, Belloni BC, Zipser MC, Schlegel NC, et al. Systematic classification of melanoma cells by phenotype-specific gene expression mapping. Pigment cell & melanoma research. 2012;25(3):343-53.
53. Kim IS, Heilmann S, Kansler ER, Zhang Y, Zimmer M, Ratnakumar K, et al. Microenvironment-derived factors driving metastatic plasticity in melanoma. Nature communications. 2017;8:14343.
54. Ganeshaiah KN, Shaanker RU. Seed Size Optimization in a Wind Dispersed Tree Butea-Monosperma - a Trade-Off between Seedling Establishment and Pod Dispersal Efficiency. Oikos. 1991;60(1):3-6.
55. Huang FF, Peng SL, Chen BM, Liao HX, Huang QQ, Lin ZG, et al. Rapid evolution of dispersal-related traits during range expansion of an invasive vine Mikania micrantha. Oikos. 2015;124(8):1023-30.
56. Williams JL, Kendall BE, Levine JM. Rapid evolution accelerates plant population spread in fragmented experimental landscapes. Science. 2016;353(6298):482-5.
57. Fronhofer EA, Altermatt F. Eco-evolutionary feedbacks during experimental range expansions. Nature communications. 2015;6:6844.
58. Lange R, Marshall DJ. Propagule size and dispersal costs mediate establishment success of an invasive species. Ecology. 2016;97(3):569-75.
59. Agostinho AA, Suzuki HI, Fugi R, Alves DC, Tonella LH, Espindola LA. Ecological and life history traits of Hemiodus orthonops in the invasion process: looking for clues at home. Hydrobiologia. 2015;746(1):415-30.
60. Simmons AD, Thomas CD. Changes in dispersal during species' range expansions. Am Nat. 2004;164(3):378-95.
61. Ochocki BM, Miller TE. Rapid evolution of dispersal ability makes biological invasions faster and more variable. Nature communications. 2017;8:14315.
62. Weiss-Lehman C, Hufbauer RA, Melbourne BA. Rapid trait evolution drives increased speed and variance in experimental range expansions. Nature communications. 2017;8:14303.
63. Hughes CL, Hill JK, Dytham C. Evolutionary trade-offs between reproduction and dispersal in populations at expanding range boundaries. Proceedings Biological sciences / The Royal Society. 2003;270 Suppl 2:S147-50.
64. Fraebel DT, Mickalide H, Schnitkey D, Merritt J, Kuhlman TE, Kuehn S. Environment determines evolutionary trajectory in a constrained phenotypic space. eLife. 2017;6.
65. Phillips BL, Brown GP, Shine R. Evolutionarily accelerated invasions: the rate of dispersal evolves upwards during the range advance of cane toads. Journal of evolutionary biology. 2010;23(12):2595-601.
66. Perkins TA, Phillips BL, Baskett ML, Hastings A. Evolution of dispersal and life history interact to drive accelerating spread of an invasive species. Ecol Lett. 2013;16(8):1079-87.
67. Hallatschek O, Fisher DS. Acceleration of evolutionary spread by long-range dispersal. Proceedings of the National Academy of Sciences of the United States of America. 2014;111(46):E4911-9.
68. Travis JMJ, Dytham C. Dispersal evolution during invasions. Evol Ecol Res. 2002;4(8):1119-29.

69. Stevens VM, Whitmee S, Le Galliard JF, Clobert J, Bohning-Gaese K, Bonte D, et al. A comparative analysis of dispersal syndromes in terrestrial and semi-terrestrial animals. Ecol Lett. 2014;17(8):1039-52.

Supplemental Information

SI Appendix 1: Material and Methods

Transplantation

The transplantation assay is performed as the following:

Wild-type swarming colony: Swarming plates are made as previously described [1]. *Pseudomonas aeruginosa* PA14 (genetically modified to constitutively express DsRed proteins) are grown in LB overnight, washed twice in Phosphate Buffered Saline (PBS), then diluted in PBS to OD600=0.01. The plate is seeded with 2 μL of bacterial solution and kept at 37°C for 20h.

Hyperswarmer liquid culture: Overnight culture of hyperswarmers (clone 4) [2] genetically modified to constitutively express GFP proteins is washed twice in PBS and concentrated 100-fold by centrifugation.

Implantation: For each plate, the location of the tip of every branch is marked on the bottom side of the Petri dish. The implant sites are marked as well. A small volume of hyperswarmers culture (0.1-0.8 μL) is implanted at each implant site. From 6 to 11 branches are implanted per swarming colony. The entire procedure takes less than 5 minutes per plate.

Implant size measurement: Immediately after implantation, each plate is placed inside a 37°C incubator containing a custom-made fluorescence imaging device. Two images are taken with the same light source (Blue LED equipped with a 500nm excitation filter): one with a 510nm emission filter (GFP channel), one without emission filter (brightfield channel). The camera dark noise and illumination unevenness are canceled out using this formula:

$$\text{Final image} = \frac{\text{GFP} - \text{dark noise}}{\text{brightfield} - \text{dark noise}}$$

The size of each implant is manually evaluated from the total GFP signal within a region defined by thresholding. In order to make the experimental results comparable with simulations, this size is divided by the area of a circle of diameter of λ_{WT}. This gives the density of GFP if the implant sites were $2\lambda_{WT}$ in diameter. Then we divide this density by the wild-type carrying capacity. To evaluate the local carrying capacity of the wild-type colony (K_{exp}), we grew a swarming colony with a wild-type mutant constitutively expressing GFP proteins, took an image using the same imaging device and performing the same post-acquisition treatment, and measured the average intensity of the branches.

Invasion outcome measurement: 6 hours after implantation, plates are imaged with a plate scanner (GE Healthcare Typhoon) in DsRed and GFP channels. The distance between the implant site and the location of the tip of the branch at the time of implantation is measured with ImageJ. The invasion outcome is estimated visually. The amount of hyperswarmers at the front of the branch is visually ranked in four levels:

- "No invasion": no visible trace of hyperswarmers at the edge of the colony (red dots in Figure 3).

- "Scarce invasion": a streak of hyperswarmers reached the edge (orange dots in Figure 3).
- "Abundant invasion": hyperswarmers settled at the tip and along the edge of the branch (yellow dots in Figure 3).
- "Full invasion": hyperswarmers took over the ancestral population and disrupted the branch pattern (green dots in Figure 3).

Growth curves

Overnight cultures of wild-type and hyperswarmer cells are washed in PBS and diluted in minimum media with casaamino acids (it is the same recipe as the one used for swarming plates except agar is removed). Cells are grown in a 96-well plate in a plate scanner (Tecan) with 37°C incubation and agitation.

Competition experiment

Overnight cultures of wild-type DsRed and hyperswarmer GFP cells are washed in PBS and mixed to an approximate 1:1 ratio. To evaluate the pre-competition ratio, a sample of this mix solution is serially diluted in PBS and inoculated on a minimum media hard agar plate for CFU counting. 1 mL of the mix solution mixture is poured on a fresh swarming plate. Once the plate is dry, it is incubated at 37°C for 4 hours. Finally, to evaluate the post-competition ratio, a small sample of the gel is scooped out using the wide side of a 1 mL sterile pipette tip to punch through the gel. The sample is placed in an Eppendorf tube with 0.5 mL of PBS, pipetted up and down 10 times to break the agar gel apart, vortexed for 10 seconds, then serially diluted in PBS and inoculated on a minimum media hard gar plate for CFU counting. 24 hours later CFU plates are scanned on a flatbed fluorescence scanner (Typhoon, GE Healthcare). 3 competition plates (per color combination) are made per day (technical replicates). This experiment is performed 3 times (biological replicates).

Numerical simulations

The deterministic numerical simulations are performed in MATLAB (The MathWorks) following Euler's method, with dx=0.1, dt=0.001, the total spatial range is 400, $D_1 = 1$ and $\mu_1 = 1$. Stochastic simulations are described below.

SI Appendix 2: Analytical solution for the condition of invasion

Formulation of the mathematical model

The traveling wave, solution of the F-KPP equation, is driven by growth at the edge of the population range. In the figure above, the population density u is represented in red, the growth limiting resources (proxied by the difference between the carrying capacity and the population density) $1-u$ in light blue, the growth $ru(1-u)$ in dark blue. The *active layer* – the region where local growth rate is at least above half the maximum rate – spans $\sim 6.8\lambda$, with $\lambda = \sqrt{D/r}$. The black arrow depicts the direction of expansion.

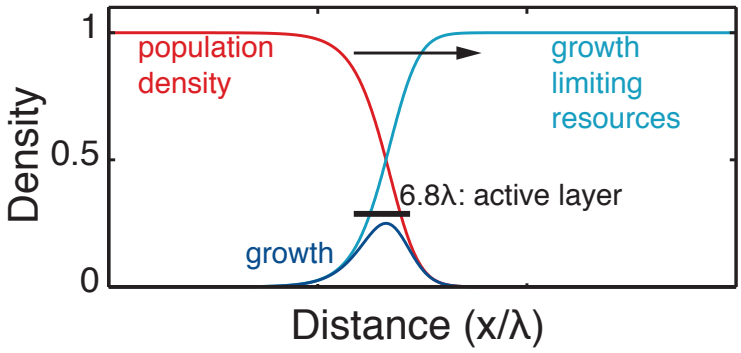

We model the density of the two species (densities u_1 and u_2) by two coupled F-KPP equations with different growth rates (r_1 and r_2) and different diffusion rates (D_1 and D_2). The two species interact only by competing for common resources.

$$\begin{aligned}\frac{\partial u_1}{\partial t} &= r_1 u_1(1-u_1-u_2) + D_1\frac{\partial^2 u_1}{\partial x^2}\\ \frac{\partial u_2}{\partial t} &= r_2 u_2(1-u_1-u_2) + D_2\frac{\partial^2 u_2}{\partial x^2}\end{aligned} \tag{S1}$$

We aim to define the range of parameters (D_1, D_2, r_1, r_2) that allow the invasion of an established traveling wave (species 1) by another species (species 2).

Eigenvalue problem

We reproduce the same arguments as in ref. [3] but with $r_1 \neq r_2$. We introduce the functions $u(t,x) = u_1(t,x) + u_2(t,x)$, $g_1(t,x) = r_1(1-u(t,x))$ and $g_2(t,x) = r_2(1-u(t,x))$.

$$\begin{aligned}\frac{\partial u_1}{\partial t} &= g_1(u)u_1 + D_1\frac{\partial^2 u_1}{\partial x^2}\\ \frac{\partial u_2}{\partial t} &= g_2(u)u_2 + D_2\frac{\partial^2 u_2}{\partial x^2}\end{aligned} \tag{S2}$$

To find the condition of invasion, we search for the condition of divergence of the fraction of secondary species:

$$f(t,x) = \frac{u_2(t,x)}{u_1(t,x)+u_2(t,x)} \tag{S3}$$

Korolev (in ref. [3]) assumes $f \ll 1$ and demonstrates that the condition of invasion can be found by solving an eigenvalue problem. Following the exact same steps, we find that in the moving reference frame (where the space variable is $\xi = x - v_1 t$) traveling at the velocity $v_1 = 2\sqrt{r_1 D_1}$ the eigenvalue problem is the following:

$$\tilde{r}f = D_2 f'' + (v_1 + 2D_2\frac{c'}{c})f' + (D_2 - D_1)\frac{c''}{c}f + (g_2 - g_1)f \tag{S4}$$

where primes denote the derivative with respect to ξ, and $\tilde{r}$ is an eigenvalue. After another change of variables established by Korolev, equation S4 is written as

$$\tilde{r}\psi = D_2\psi'' + \Big(g_2(c) - \frac{v_1^2}{4D_2}\Big)\psi \tag{S5}$$

Condition of invasion

Following Korolev's reasoning [3], we find that the largest eigenvalue is found at large ξ (far in front of the wave, where u is small), and its value is given by the maximal value of $g_2(c)$:

$$\begin{aligned} \tilde{r}_{\max} &= r_2 - \frac{v_1^2}{4D_2} \\ &= \frac{v_2^2 - v_1^2}{4D_2} \end{aligned} \tag{S6}$$

If $\tilde{r}_{\max} < 0$ then the secondary species will never invade the primary species. If $\tilde{r}_{\max} > 0$ then the secondary species will eventually invade the primary species. Therefore, the condition of invasion corresponds to

$$v_2 > v_1 \tag{S7}$$

with $v_1 = 2\sqrt{r_1 D_1}$ and $v_2 = 2\sqrt{r_2 D_2}$.

SI Appendix 3: Time of invasion

The equation S7 gives the condition of invasion, but not the time of invasion, which depends on the size S of the introduced population and the location of the introduction (distance L from the front).

Definitions of S and L

We first consider a traveling wave formed by the species 1. Then the species 2 is introduced at a distance L from the population front, as depicted in the figure below. The front position is defined as the location where u_1 is equal to 5% of the carrying capacity. This threshold is arbitrarily selected but it is not essential for later conclusions. The position of the front at the time of introduction can be taken as the origin of the x-axis, and the time of the introduction sets the origin of time (i.e. $u_1(0,0) = 0.05$). The introduction imposes a density $u_2(x,0) = S$ for $-L-\lambda_1 < x < -L+\lambda_1$, and $u_2(x,0) = 0$ everywhere else ($\lambda_1 = \sqrt{D_1/r_1}$). Then we consider the F-KPP processes for both species simultaneously. We set $r_1 = 1$ and $D_1 = 1$ by rescaling space ($x \to x/\lambda_1$) and time ($t \to r_1 t$): the remaining parameters are D_2 and r_2. The time of invasion t_i at which the species 2 takes over the species 1 at the front is defined by:

$$u_2(x_f, t_i) > u_1(x_f, t_i) \tag{S8}$$

with the position of the front defined as

$$u_1(x_f, t) + u_2(x_f, t) = 0.05 \tag{S9}$$

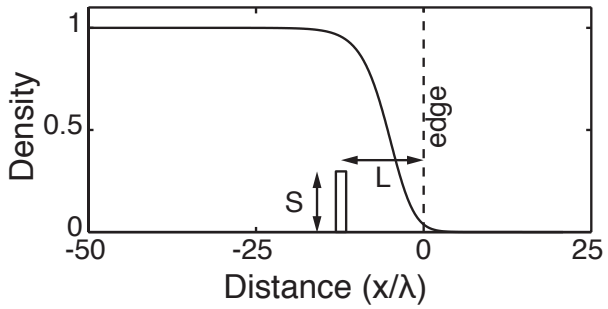

An approximate time of invasion can be calculated by considering the invasion in two consecutive steps. First, the introduced individuals of species 2 spread through spatial diffusion until the density f of species 2 at the edge reaches a maximum. During this step we assume that species 2 does not grow. Then, the individuals of species 2 that reached the edge contribute to the traveling wave. They have access to the resources and therefore they proliferate until they take over the species 1.

Diffusive spreading

The introduced population (species 2) is initially spatially limited, and performed at $x = 0$, at distance L from the edge. Then it diffuses out, and its density is:

$$u_2(x,t) = N_2^0 \frac{e^{-\frac{x^2}{4D_2 t}}}{\sqrt{4\pi D_2 t}} \tag{S10}$$

where N_2^0 is the total size of the introduced population. To compare the theoretical and experimental results, we rescale the total size of the introduced population using its spatial extension:

$$N_2^0 = 2\lambda_1 S \tag{S11}$$

The density of species 2 at the edge of the traveling wave formed by species 1 is $u_2(x = v_1 t + L, t)$ and it reaches a maximum at

$$t = t_{\text{diffusion}} \equiv \frac{\sqrt{D_2^2 + v_1^2 L^2} - D_2}{v_1^2} \tag{S12}$$

At this time, the density of species 2 at the edge is

$$u_{2,\text{diffusion}} = 2\lambda_1 S \frac{e^{-\frac{(v_1 t_{\text{diffusion}} + L)^2}{4 D_2 t_{\text{diff}}}}}{\sqrt{4\pi D_2 t_{\text{diff}}}} \tag{S13}$$

Since the edge of the population range is defined as the location where the total density is 5% of the carrying capacity, the fraction of species 2 at the edge is

$$f_{\text{diffusion}} = \frac{2\lambda_1 S}{0.05} \frac{e^{-\frac{(v_1 t_{\text{diffusion}} + L)^2}{4 D_2 t_{\text{diffusion}}}}}{\sqrt{4\pi D_2 t_{\text{diffusion}}}} \tag{S14}$$

Growth at the edge

At the edge, the densities of species 1 and species 2 are much smaller than the carrying capacity, so we consider that they grow exponentially. If species 1 and 2 grow exponentially with growth rates r_1 and r_2, respectively, then the evolution of the frequency f is given by the logistic equation with a growth rate $r_2 - r_1$. We study the early times of invasion, hence f remains much smaller than 1. Therefore, we simply write:

$$\frac{\partial f}{\partial t} = (r_2 - r_1) f \tag{S15}$$

Here, we study the dynamics of the frequency f in the moving reference frame at short times, so we can assume that f follows the dynamics given by the eigenvalue equation S4 and therefore grows at a rate corresponding to the maximal eigenvalue given in equation S6. Then we can replace $r_2 - r_1$ with $\tilde{r}_{\max}$ in equation S15.

The dynamics of f is therefore:

$$f(t) = f_{\text{diffusion}} e^{\tilde{r}_{\max} t} \tag{S16}$$

Frequency of species 2 at the edge

If the introduction is performed far enough from the edge ($L > D_2/v_1$), then equation S12 becomes simply $t_{\text{diffusion}} \simeq L/v_1$ and equation S14 becomes:

$$\begin{aligned} f_{\text{diffusion}} &\simeq \frac{2\lambda_1 S}{0.05} \frac{e^{-\frac{L v_1}{D_2}}}{\sqrt{4\pi D_2 L / v_1}} \\ &\simeq \frac{S}{0.05} \frac{1}{\sqrt{\pi}} \sqrt{\frac{D_1}{D_2}} \sqrt{\frac{v_1}{r_2 L}} e^{-\frac{L v_1}{D_2}} \end{aligned} \tag{S17}$$

Since the $\sqrt{L}$ evolves much more slowly then $e^{-\frac{Lv_1}{D_2}}$, we consider that L is constant in this term (we use $L = \tilde{L} = 5$mm for the experimental validation):

$$f_{\text{diffusion}} \simeq \frac{S}{0.05}\frac{1}{\sqrt{\pi}}\sqrt{\frac{D_1}{D_2}}\sqrt{\frac{v_1}{r_2\tilde{L}}}e^{-\frac{Lv_1}{D_2}} \tag{S18}$$

The frequency of species 2 after a time t is given by equation S16 but using the shifted time $t - t_{\text{diffusion}}$ that accounts for the time required for species 2 to reach the edge.

$$\begin{aligned} f(t) &\simeq \frac{S}{0.05}\frac{1}{\sqrt{\pi}}\sqrt{\frac{D_1}{D_2}}\sqrt{\frac{v_1}{r_2\tilde{L}}}e^{-\frac{Lv_1}{D_2}}e^{\tilde{r}_{\max}(t-t_{\text{diffusion}})} \\ &\simeq \frac{S}{0.05}\frac{1}{\sqrt{\pi}}\sqrt{\frac{D_1}{D_2}}\sqrt{\frac{v_1}{r_2\tilde{L}}}e^{\frac{v_2^2-v_1^2}{4D_2}t}e^{-\frac{3v_1^2+v_2^2}{4D_2v_1}L} \end{aligned} \tag{S19}$$

Hence the iso-frequency lines in Figure 3A are given by $S \sim e^{L/L_0}$, with $L_0 = \frac{4D_2v_1}{3v_1^2+v_2^2}$ (equation 5 of the main text).

The iso-frequency for $f = 0.25$ is plotted in the figure below (red dashed line), together with the numerical results. The disagreement with the numerical results is mostly due to the simplicity of the model: first the species 2 diffuses out and reaches a maximum density at the edge, then it grows at the edge. In reality, species 2 starts growing as soon as it approaches the edge and gains access to resources. To account for this neglected growth term, we propose a simple correction: we replace the frequency at the edge $f_{\text{diffusion}}$ with $f_{\text{diffusion}}(1 + t_{\text{diffusion}}r_2/2)$ in equation S16. The term $f_{\text{diffusion}}t_{\text{diffusion}}r_2/2$ comes from the approximate integration of the growth of the frequency f at the edge from $t = 0$ ($f = 0$) to $t = t_{\text{diffusion}}$ ($f = f_{\text{diffusion}}$). Including this growth term improves the agreement with the numerical simulations (red solid line of the figure below).

Time of invasion

If $L > D_2/v_1$, the time of diffusion from implantation to the edge is

$$t_{\text{diffusion}} \simeq L/v_1 \tag{S20}$$

The time of growth t_{growth} to reach a certain frequency f is:

$$\begin{aligned} t_{\text{growth}} &\simeq \frac{1}{\tilde{r}_{\max}}\log\left(\frac{f}{f_{\text{diffusion}}}\right) \\ &\simeq \frac{1}{\tilde{r}_{\max}}\left(\log(0.05f/S) + \frac{1}{2}\log(\frac{\pi r_2\tilde{L}D_2}{D_1v_1}) + \frac{Lv_1}{D_2}\right) \end{aligned} \tag{S21}$$

Overall, the time of invasion $t_i = t_{\text{diffusion}} + t_{\text{growth}}$ scales as (equation 4 of the main text):

$$t_i \sim \alpha L - \beta\log(S) \tag{S22}$$

with

$$\begin{aligned} \alpha &= \frac{4v_1}{v_2^2 - v_1^2} \\ \beta &= \frac{4D_2}{v_2^2 - v_1^2} \end{aligned} \tag{S23}$$

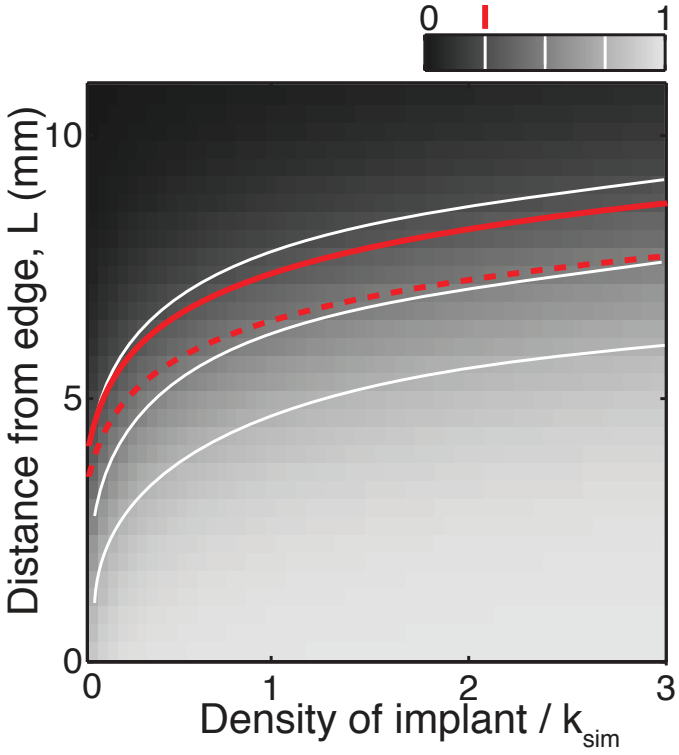

Figure: Comparison between numerical and theoretical results. The color scale represents the simulated score of invasion (the ratio f of species 2 density over total population density) at the front of the expansion range, at $t = 6$ hours after implantation. The secondary species is characterized by $D_2 = 2D_1$ and $r_2 = 0.9r_1$. The white lines are iso-frequency contour lines for simulated score $f = 0.25$, 0.5, and 0.75. The red dashed line is the $f = 0.25$ contour line from equation S19. The red solid line is the $f = 0.25$ contour line corrected for growth.

SI Appendix 4: Stochastic modeling

The model presented above is deterministic. We introduce stochasticity by updating species counts N_1 and N_2 using distribution functions based on equations S1.

Logistic Growth

At each time step, the counts of species 1 and 2 are updated to account for logistic growth:

$$\begin{aligned} N_1(x, t + dt) &\to N_1(x, t) + \text{Poisson}(r_1\, dt\, N_1(x, t)(1 - N_1(x, t)/K - N_2(x, t)/K)) \\ N_2(x, t + dt) &\to N_2(x, t) + \text{Poisson}(r_2\, dt\, N_2(x, t)(1 - N_2(x, t)/K - N_2(x, t)/K)) \end{aligned} \tag{S24}$$

where Poisson(λ) is the Poisson distribution function, with parameter λ.

Exponential Growth + Death

To introduce a net death rate, we develop the expression of the deterministic logistic growth into a (positive) exponential growth term and a (negative) density dependant death term.

$$\begin{aligned} r_1 N_1(1 - \frac{N_1}{K} - \frac{N_2}{K}) &= r_1 N_1 - r_1 N_1 (N_1 + N_2)/K \\ r_2 N_2(1 - \frac{N_1}{K} - \frac{N_2}{K}) &= r_2 N_2 - r_2 N_2 (N_1 + N_2)/K \end{aligned} \tag{S25}$$

Therefore, at each time step, species counts are updated in the following way:

$$\begin{aligned} &N_1(x, t + dt) \to N_1(x, t) + \text{Poisson}(r_1\, dt\, N_1(x, t)) \\ &N_1(x, t + dt) \to N_1(x, t) - \text{Binomial}(N_1(x, t), r_1\, dt (N_1(x, t) + N_2(x, t))/K) \\ &N_2(x, t + dt) \to N_2(x, t) + \text{Poisson}(dt\, r_2 N_2(x, t)) \\ &N_2(x, t + dt) \to N_2(x, t) - \text{Binomial}(N_2(x, t), r_2\, dt (N_1(x, t) + N_2(x, t))/K) \end{aligned} \tag{S26}$$

where Binomial(n, p) is the binomial distribution function, with parameters n (number of trials) and p (success probability in each trial).

Diffusion

At each time step, a random fraction of individuals of species 1 at deme x are randomly moved into demes $x + dx$ and $x - dx$. All demes are processed sequentially in a random order with the following scheme:

- draw $B = \text{Binomial}(N_1, p = D_1\, dt\, /\, dx^2)$
- draw $B_{\text{left}} = \text{Binomial}(B, p = 0.5)$. Then $B_{\text{right}} = B - B_{\text{left}}$.
- update $N_1(x, t + dt) \to N_1(x, t) - B$
- update $N_1(x - dx, t + dt) \to N_1(x - dx, t) + B_{\text{left}}$
- update $N_1(x + dx, t + dt) \to N_1(x + dx, t) + B_{\text{right}}$

Diffusion is performed in a similar way for species 2.

In practice, we set $dt = 1$ and $dx = 1$ without loss of generality. We also keep r_1, r_2, D_1, and D_2 small enough to ensure that the probabilities in binomial distributions remain smaller than one.

Evolutionary simulations without trade-off

At each time point, each division gives rise to a mutation with a probability of 5%. Each new phenotype is randomly drawn from a normal distribution centered on the ancestor phenotype, with a standard deviation of 0.1 times the phenotype in each direction. To speed up the simulations, subpopulations that did not reach a certain size after a certain time since they appeared are cleared up and their counts are randomly distributed over the remaining populations.

Evolutionary simulations with trade-off

At each time point, each division gives rise to a mutation with a probability of 1%. Each new phenotype randomly falls on the trade-off line (uniform distribution), which is splitted into 500 bins within the first quadrant of the space (r, D).

SI Appendix 5: Statistical analysis

Figure 3C

To study the shape of the four classes of invasion in the density-distance space (Figure 3C), we performed a classification with a multinomial logistic regression. Each boundary between two adjacent classes is tested independantly. In practice, we used the function *mnrfit* of MATLAB to fit the data with a power law model.

$$Class = a_0 + a_1 \log(Density) + a_2 \log(Distance) \tag{S27}$$

where *Class* is 0 or 1 for each of the two tested classes.

The boundary between the two classes is defined by $Class = 0.5$:

$$Distance = \exp(\frac{0.5 - a_0}{a_2}) Density^{-a_1/a_2} \tag{S28}$$

The exponent $(-a_1/a_2)$ is lower than 1 (with statistical significance reported in the table below, the brackets represent 95% confidence intervals which are calculated from standard deviations calculated by the multinomial logistic regression and combined using Fieller's theorem) in the three cases indicating that boundaries between classes have a concave shape, in agreement with the the 2-species FKPP model (Figure 3A).

Boundary	exponent [95% confidence interval]
no invasion - scarce invasion	0.24 [0.11, 0.38]
scarce invasion - abundant invasion	0.43 [0.22, 0.63]
abundant invasion - full invasion	0.57 [0.27, 0.88]

Figure S2

Figure S2 shows the results of the competition wild-type vs hyperswarmer on a plate when the spatial structure is suppressed. The wild-type outcompetes the hyperswarmer mutant. The significance of this result is estimated using a generalized linear model for binomial data (function *fitglm.m* in MATLAB). We used the formula $c \sim 1 + f + (1|R) + (f|S)$, where c is the wild-type count, f is the categorical variable 'before competition' or 'after competition', R is the replicate index, and S is the color index (we performed the two types of experiments: wild-type GFP vs. hyperswarmer DsRed, and wild-type DsRed vs. hyperswarmers GFP). The fit gave a p-value $= 4.5 \times 10^{-5}$.

SI Appendix 6: Supplemental References

[1] Xavier, J. B., Kim, W. & Foster, K. R. A molecular mechanism that stabilizes cooperative secretions in Pseudomonas aeruginosa: Metabolic prudence in P. aeruginosa. *Molecular Microbiology* **79**, 166–179 (2011). URL `http://doi.wiley.com/10.1111/j.1365-2958.2010.07436.x`.

[2] van Ditmarsch, D. *et al.* Convergent Evolution of Hyperswarming Leads to Impaired Biofilm Formation in Pathogenic Bacteria. *Cell Reports* **4**, 697–708 (2013). URL `http://linkinghub.elsevier.com/retrieve/pii/S2211124713003884`.

[3] Korolev, K. S. Evolution Arrests Invasions of Cooperative Populations. *Physical Review Letters* **115** (2015). URL `http://link.aps.org/doi/10.1103/PhysRevLett.115.208104`.

[4] Deforet, M., van Ditmarsch, D. & Xavier, J. B. Cell-size homeostasis and the incremental rule in a bacterial pathogen. *Biophysical Journal* **109**, 521–528 (2015).

[5] Deforet, M., van Ditmarsch, D., Carmona-Fontaine, C. & Xavier, J. B. Hyperswarming adaptations in a bacterium improve collective motility without enhancing single cell motility. *Soft Matter* **10**, 2405 (2014). URL `http://xlink.rsc.org/?DOI=c3sm53127a`.

SI Appendix 7: Supplemental Figures

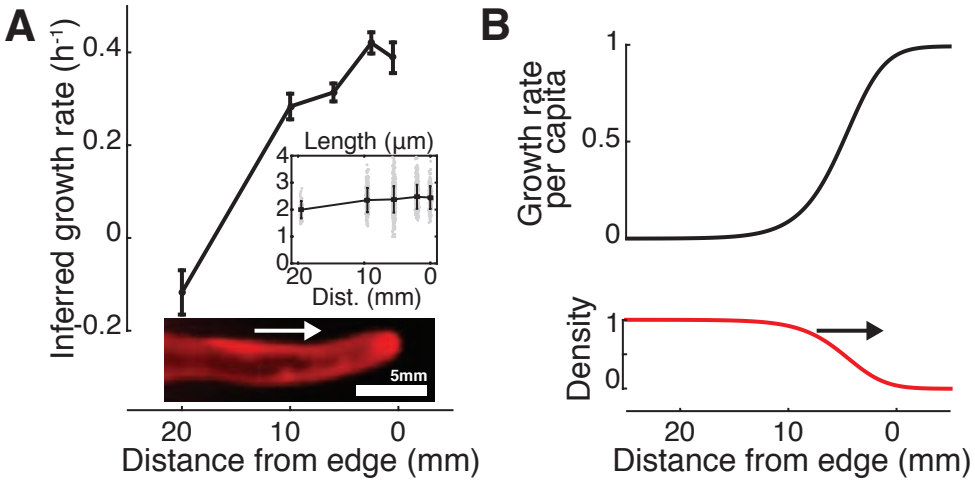

Figure S1: **Bacterial swarming can be modeled by FKPP equation where growth is greatest at the edge.** A: The length of each bacterium is converted into a growth rate, using the results of a previous study [4] linking cell length to growth rate, where this fit is obtained: $L = 2.18 + 0.89\mu$ (L is the length of a bacterium and μ is its growth rate). Errors bars are standard error of the mean ($N \simeq 100$). Inset: Cells length measured by fluorescent microscopy and automated image analysis. Error bars are standard deviations. Data points are randomly distributed around each value of distance (X-axis) for better visualization. The bottom picture represents a wild-type branch growing on soft agar gel. The white arrow depicts the direction of expansion. B: The growth rate per capita ($r(1-u)$, with $r = 1$, black line), and the density (u) of the population simulated by the FKPP equation (black line). The black arrow depicts the direction of expansion.

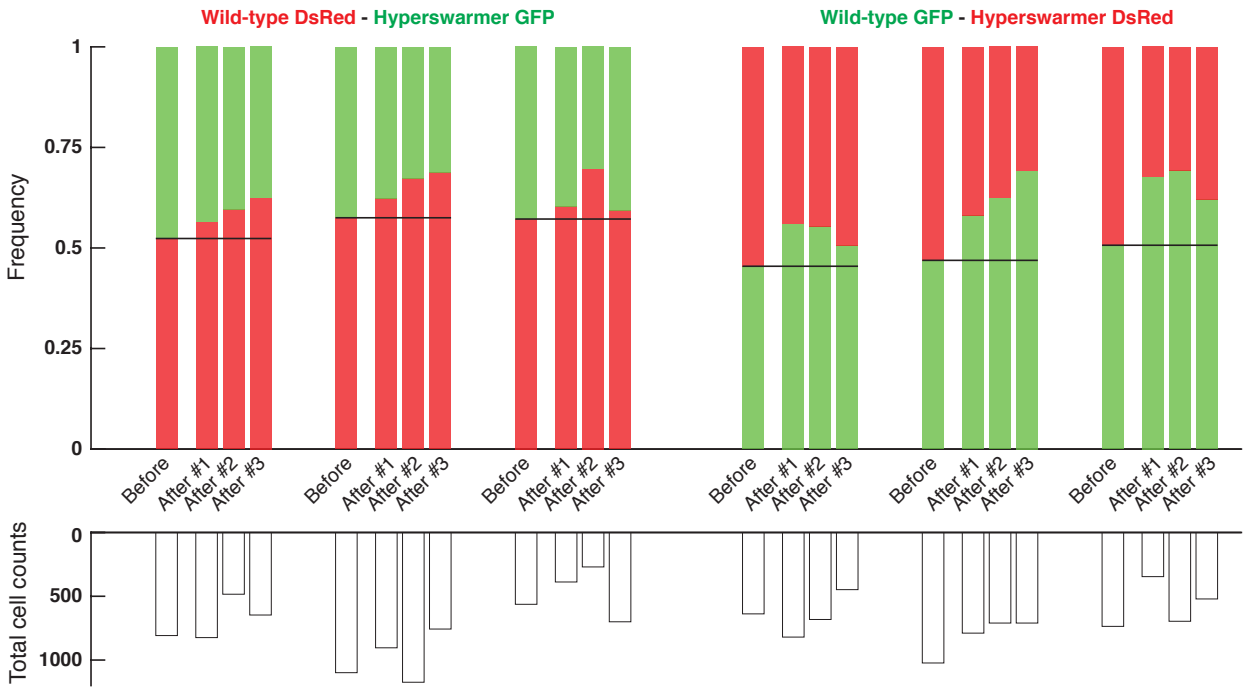

Figure S2: **Wild-type *P. aeruginosa* outcompetes its hyperswarmer mutant on a plate when the spatial structure is suppressed.** Swarming plates (0.5% agar) are inoculated with a loan of a mixed population of wild-type and hyperswarmers (approximate initial ratio 1:1) and incubated for 4 hours of incubation at 37°C. The ratios of wild-type before and after the competition are estimated using CFUs counting. GFP and DsRed fluorescent proteins (constitutively expressed) are used to take apart the two bacterial strains. Swapped experiments confirm that despite toxicity of DsRed proteins, wild-type cells outcompete hyperswarmers ($p = 4.5 \times 10^{-5}$, generalized linear model for binomial data). N=3 biological replicates x 3 technical replicates per color combination.

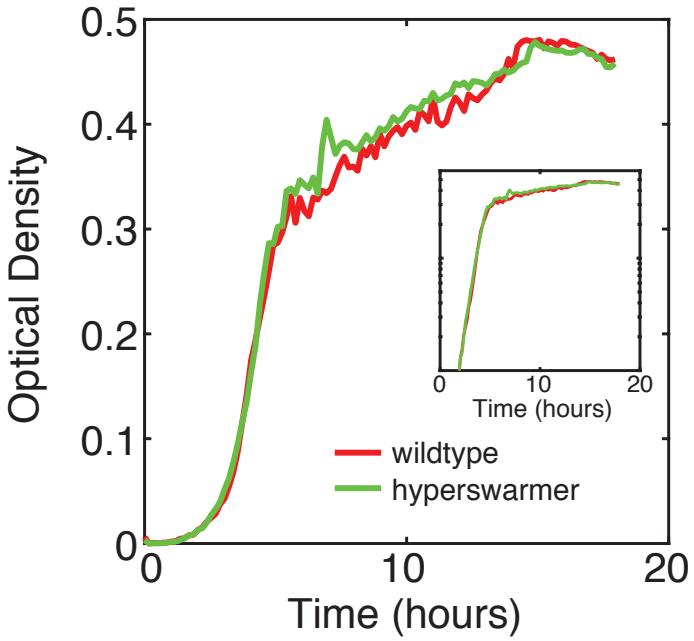

Figure S3: **Wild-wild-typetype *P. aeruginosa* and its hyperswarmer mutant have comparable carrying capacities.** The bacterial density is measured in a plate scanner as optical density. Inset: Growth curves in logarithmic scale.

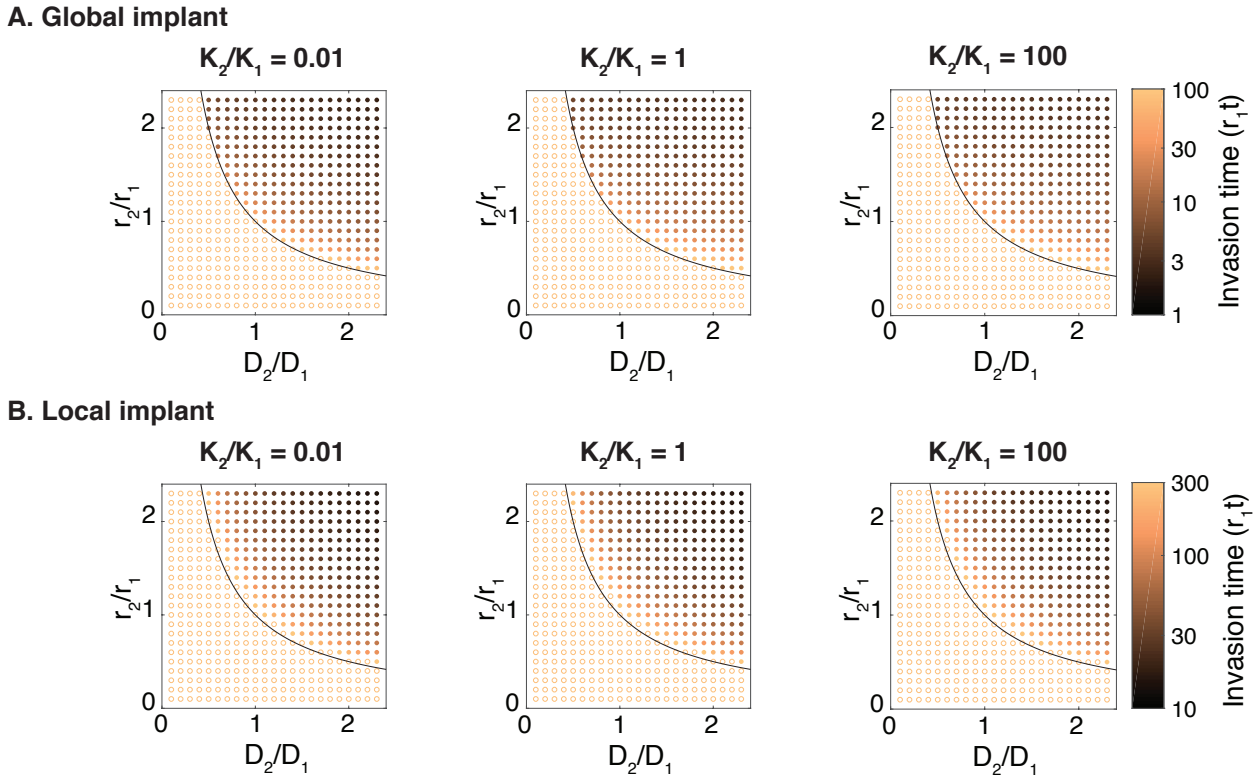

Figure S4: **Carrying capacities don't affect the invasion processes.** A: Species 2 is introduced globally with $u_2 = u_1/100$. B: Species 2 is introduced locally with $u_2(x) = 0.2$ where $-16 < x < -14$ (with the edge of the population being at $x = 0$).

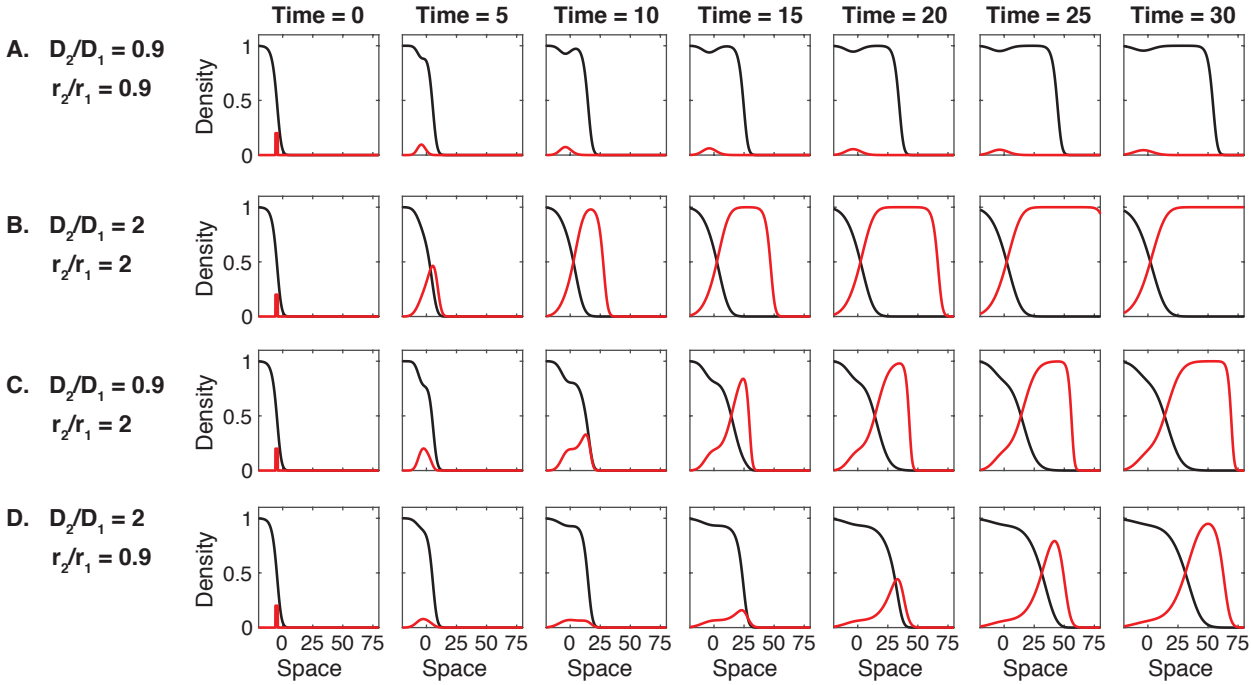

Figure S5: **Snapshots of invasion (or non-invasion) after introduction of species 2.** A: Non-invasive case with lower growth and lower dispersal. B: Invasive case with greater growth and greater dispersal. C: Invasive case with greater growth but lower dispersal. D: Invasive case with lower growth but greater dispersal. See also Movie S4.

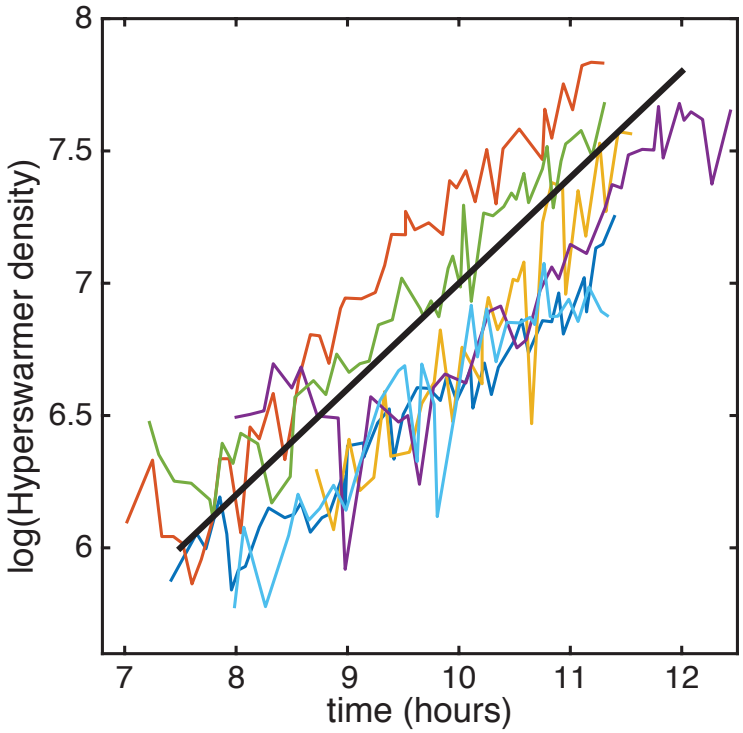

Figure S6: **Hyperswarmers density dynamics at the edge of the colony, from Movie S1.** The dynamics of the density of hyperswarmers is governed by the eigenvalue $\tilde{r}_{\max} = r_2 - \frac{v_1^2}{4D_2}$, in the limit of low density. Experimental parameters (Table S1) yields to $\tilde{r}_{\max} = 0.4$ h^{-1}. The black line is a visual guide with a rate of 0.4 h^{-1}. The average slope of the six curves is 0.39 $\pm$0.08h^{-1} (Standard deviation).

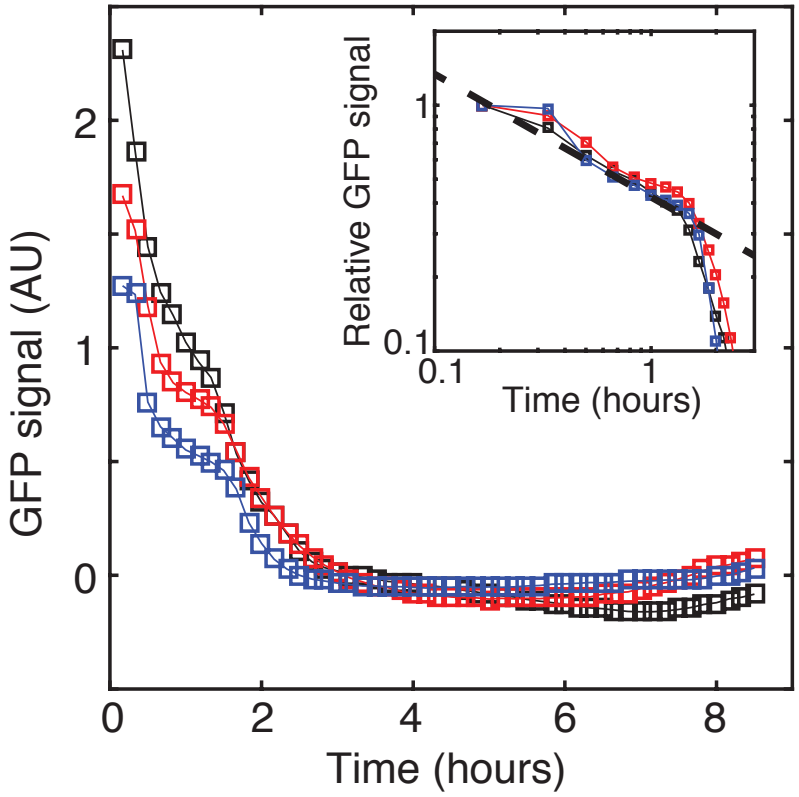

Figure S7: **Hyperswarmers introduced into a wild-type swarming colony spread by diffusion.** Three representative implant sites are analyzed. The data represents the average GFP signal at the site of introduction. GFP signal measured 1 cm closer to the center of the colony is used for background correction. Data extracted from video S5A. Inset: the first 1.5 hours can be modeled by a diffusive decay. The dashed line is the prediction from 1D diffusion decay, using $D = 4$ mm^2/h and a inoculum size of $L = 3$ mm ($C \sim \frac{C_{\max} L}{\sqrt{4\pi D t}}$).

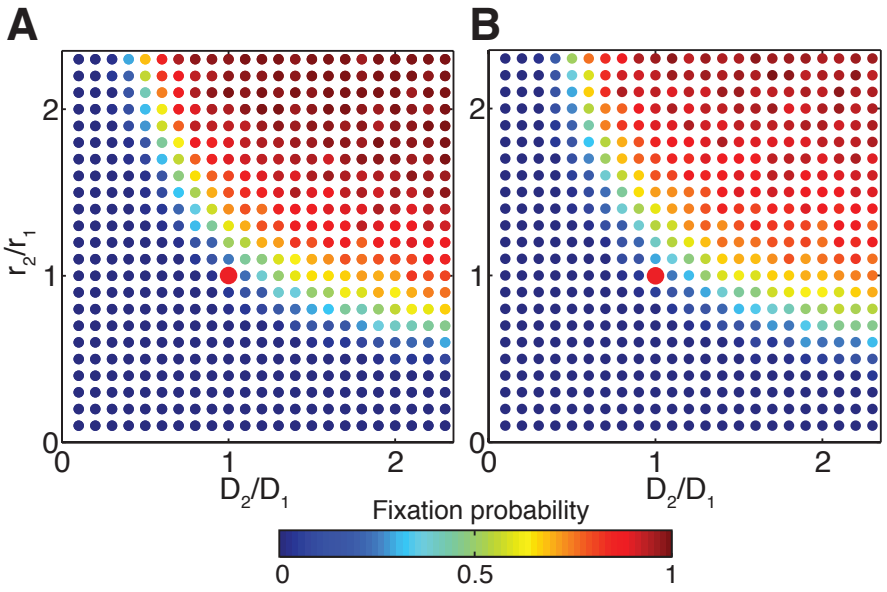

Figure S8: **Invasion diagram in stochastic models.** Fixation probability obtained from the stochastic model without death (A), and with death (B). The red dot depicts the reference point ($D_2 = D_1$ and $r_2 = r_1$). Parameters used on the simulations: $S = 1$, $K = 100$, $L = 2\lambda_1$

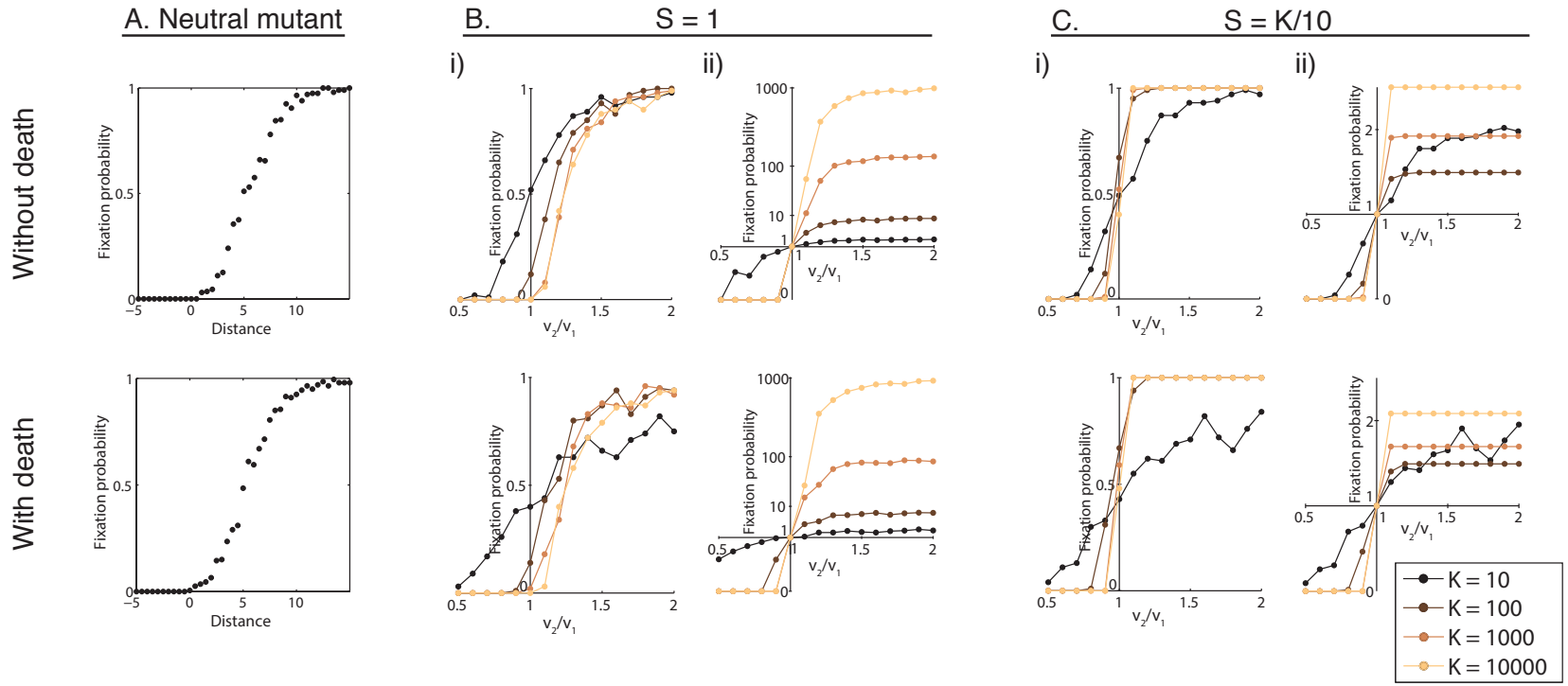

Figure S9: **Fixations probability in stochastic models.** The first row shows results of the stochastic model without death. The second row shows results of the stochastic model with death. A. Fixation probability of a neutral mutant with respect to the distance to the front ($S = 1$). B. Fixation probability of a mutant with respect to v_2/v_1 (with $r_2/r_1 = D_2/D_1$), for various carrying capacities. The introduction occurs at fixed implant size ($S = 1$ individual) at $L = 3$. i) represents the raw data in linear scale. ii) represents the data normalized by the fixation probability of a neutral mutant (note power-law scale on the y-axis, exponent=0.2). C. Fixation probability of a mutant with respect to v_2/v_1 (with $r_2/r_1 = D_2/D_1$), for various carrying capacities. Unlike in B, the number of introduced individuals scales with carrying capacity ($S = K/10$). i) represents the raw data in linear scale. ii) represents the data normalized by the fixation probability of a neutral mutant, in linear scale. Note that in B and C, for the model with and without death, the fixation probability curves get steeper as the carrying capacity gets larger.

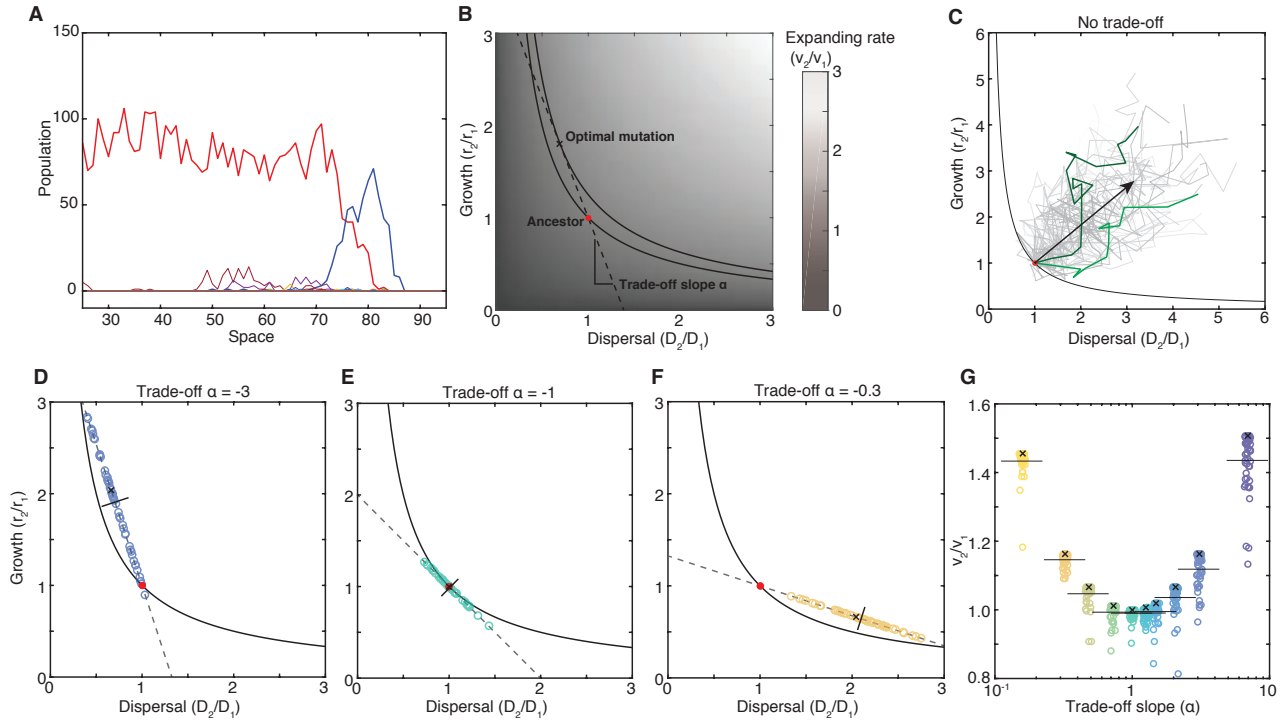

Figure S10: **Stochastic simulations of population expansion with mutations reveal that evolution tends to maximize the expansion rate $v = 2\sqrt{rD}$.** A: Representative snapshot of the spatial distributions of a population (red line) and mutant populations it has generated. B: Diagram representing the ancestral phenotype (red dot), the invasion rule (black line), a trade-off line (dashed line), the expansion rate (grey levels), and the phenotype that maximizes the expansion rate along the trade-off line (cross symbol). C: Without trade-off between growth and dispersal, evolution tends to improve both traits simultaneously. 50 evolutionary trajectories of the majority phenotype sitting at the edge are represented. Two trajectories are highlighted in green. The black arrow depicts the average trajectory (average from 50 simulations). D-E-F: Phenotypes obtained after $r_1 t = 1000$ with 3 trade-off slopes: -0.5, -1, -2. The black line is the average phenotype from 50 simulations, the cross is the theoretical optimal phenotype. G: Summary of the results for 10 trade-off slopes.

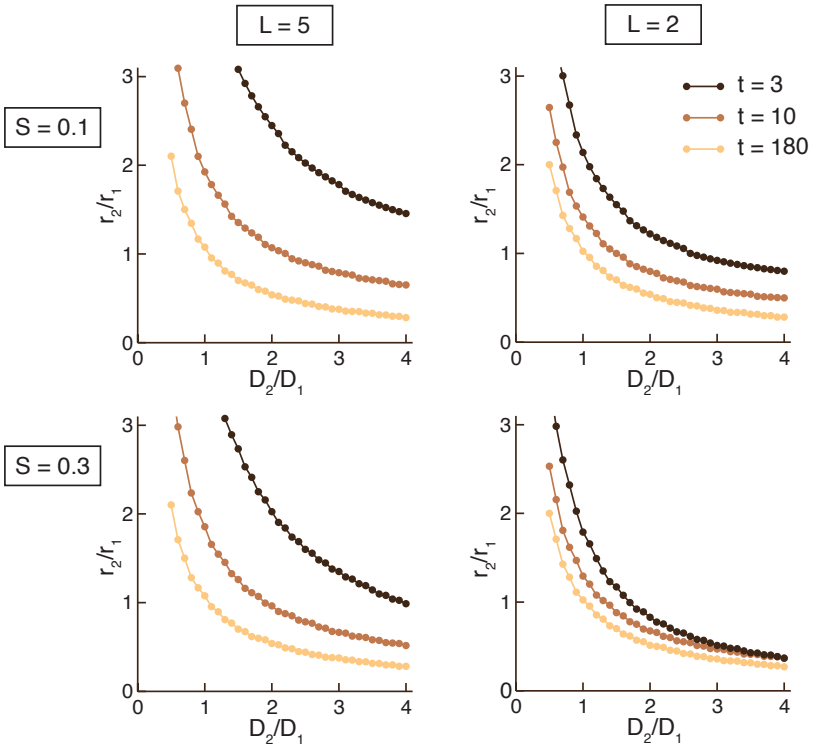

Figure S11: **Invasion domain boundaries for various simulation time, sizes of introduction S, and distances of introduction L.**

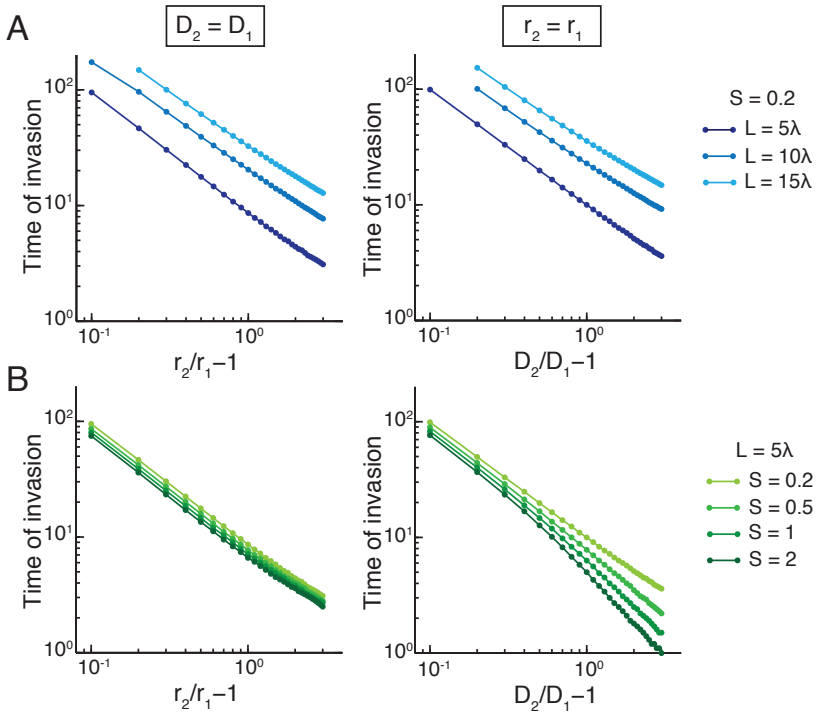

Figure S12: **Implanting further away or lower amount delays invasion.** A: Time of invasion for different implantation sites. B: Time of invasion for different implant sizes.

SI Appendix 8: Supplemental Table

Strain	Growth rate $\boldsymbol{r}$ (measured in [4])	Expansion rate $\boldsymbol{v}$ (measured in [5])	Diffusion rate $\boldsymbol{D}$ (calculated)	Decay length $\boldsymbol{\lambda}$ (calculated)
Wild-type	1.1 $\pm$0.05 h^{-1}	3.0 $\pm$0.1 mm/h	2.0 $\pm$0.15 mm^2/h	1.4 $\pm$0.07 mm
Hyperswarmer	1.0 $\pm$0.04 h^{-1}	4.0 $\pm$0.15 mm/h	4.0 $\pm$0.27 mm^2/h	2.0 $\pm$0.11 mm

Table S1: Experimental swarming traits of *Pseudomonas aeruginosa* and its hyperswarmer mutant. Errors are standard deviations. Errors on calculated parameters are inferred from the formula of propagation of errors. To simulate the invasion of hyperswarmers into wild-type colonies for the Figure 3A, we used the parameters $D_2/D_1 = 2$ and $r_2/r_1 = 0.9$.

SI Appendix 9: Supplemental Movies

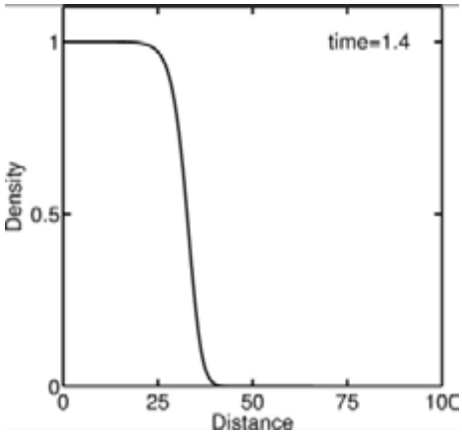

Movie S1: Traveling wave solution of the F-KPP equation, advancing at the speed $v = 2\sqrt{rD}$.

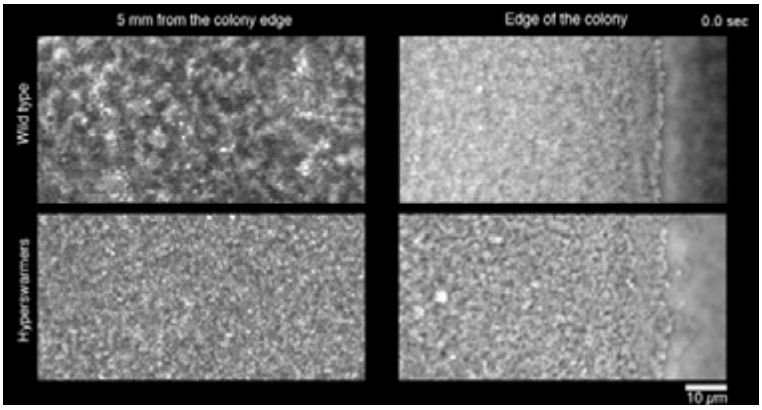

Movie S2: Phase-contrast video-microscopy images of *P. aeruginosa* swarming colonies. Top row: *P. aeruginosa* wild-type colony. Bottom row: Hyperswarmer mutant colony. Left side: 5 mm from the edge. Right side: edge of the swarming colony. Note the active turbulence patterns displayed by the hyperswarmer colony, whereas wild-type cells seem more static.

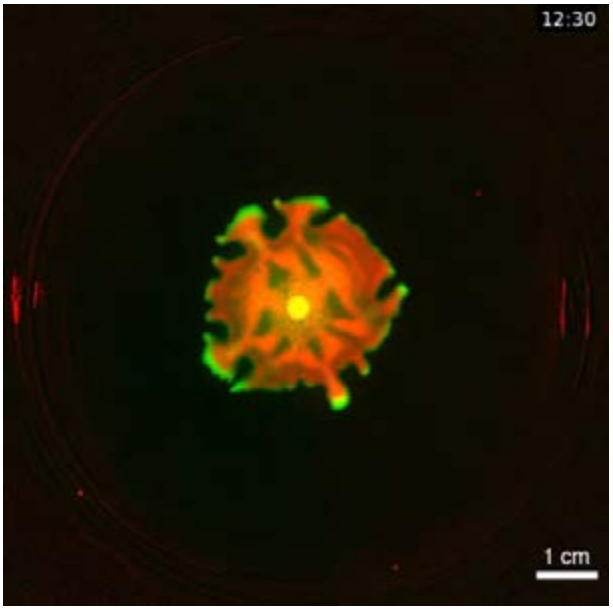

Movie S3: Fluorescence video of a swarming colony formed by a mixed population *P. aeruginosa* wild-type / Hyperswarmers (initial ratio 10:1). *P. aeruginosa* wild-type constitutively expresses DsRed (red). Hyperswarmer mutant constitutively expresses GFP (green).

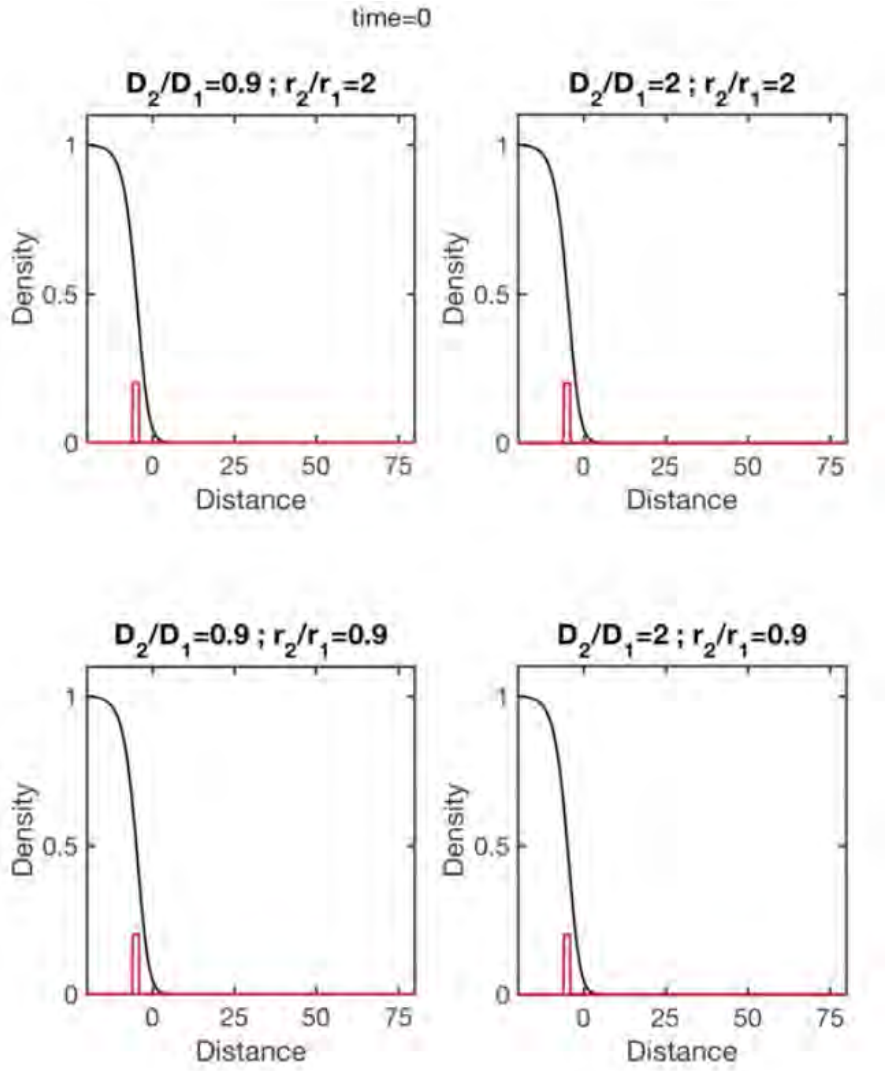

Movie S4: Invasion assay performed in numerical simulations. The black line represents the density of species 1. The red line represents species 2, implanted at t=0 at the distance L=5 from the edge.

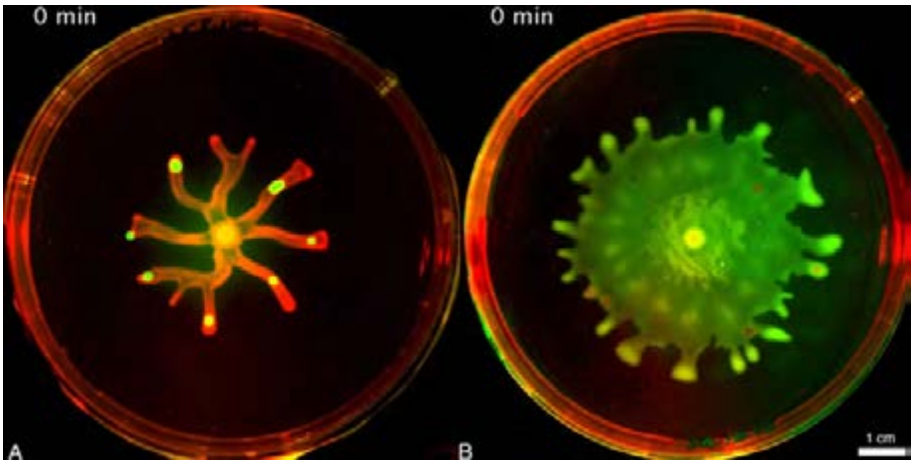

Movie S5: Implantation experiments. A: Hyperswarmers (green) are implanted into wild-type (red) swarming branches. B: Wild-type (red) are implanted into a hyperswarmer colony.